

UNIVERZA V LJUBLJANI
FAKULTETA ZA FARMACIJO

ANA PAVLOVIČ

MAGISTRSKA NALOGA

MAGISTRSKI ŠTUDIJ LABORATORIJSKA BIOMEDICINA

Ljubljana, 2014

UNIVERZA V LJUBLJANI
FAKULTETA ZA FARMACIJO

ANA PAVLOVIČ

**VLOGA ENDOCITOTSKIH POTI PRI TVORBI AGREGATOV CITOSOLNIH
PRIONOV**

**THE ROLE OF ENDOCYTOTIC PATHWAYS FOR CYTOSOLIC PRION
AGGREGATE INDUCTION**

Ljubljana, 2014

Magistrsko nalogo sem v sklopu Erasmus programa opravljala na Nemškem centru za nevrodegenerativne bolezni (Deutsches Zentrum für Neurodegenerative Erkrankungen; DZNE), pod mentorstvom prof. dr. Janka Kosa in somentorstvom prof. dr. Ine Vorberg. Visokozmogljive analize avtomatske delovne postaje in statistične obdelave podatkov reakcij glede na odmerek (dose response) so bile izvedene v sodelovanju z oddelkom za visokozmogljive analize (DZNE high content screening facility).

Mentor: prof. dr. Janko Kos,
Univerza v Ljubljani, Fakulteta za farmacijo,
Katedra za farmacevtsko biologijo

Somentorica: prof. dr. Ina Vorberg,
Universität Bonn, LIMES Institute,
Developmental biology and genetics

Komisija za oceno in zagovor

Predsednik: prof. dr. Darko Černe
Mentor: prof. dr. Janko Kos
Somentorica: prof. dr. Ina Vorberg
Član: doc. dr. Tomaž Volk

Acknowledgment/Zahvala

I would like gratefully and sincerely thank my supervisor dr. Shu Liu for her patient guidance and advices given throughout my time as her master student. Additionally I would like to thank all members of the AG Vorberg and AG Denner group for everything they taught me and for their friendly support and encouragement. Especially I would like to thank Simon for his guidance through the world of no stress and lovely moments.

Za pomoč in nasvete pri magistrskem študiju se najlepše zahvaljujem tudi pet peresni deteljici SAM NI-ja in Društvu študentov farmacije Slovenije za izjemne in nepozabne trenutke.

Izjava

Izjavljam, da sem magistrsko nalogo samostojno izdelala pod vodstvom mentorja prof. dr. Janka Kosa in somentorice prof. dr. Ine Vorberg.

Ljubljana, december 2014

Ana Pavlovič

CONTENT

1	INTRODUCTION	1
1.1	Prions – the infectious agents.....	1
1.2	Biochemical characteristics of prions	2
1.3	Prions can propagate in cell culture	5
1.4	Yeast prions.....	6
1.5	The Sup35 model system in mammalian cells.....	8
1.6	Endocytic pathways	10
2	AIM OF STUDY	13
3	HYPOTHESES.....	14
4	METHODS AND MATERIAL.....	15
4.1	Biological Safety.....	15
4.2	Protein biological analysis	15
4.2.1	Transformation and cultivation of <i>E. coli</i> with plasmid DNA.....	15
4.3	Isolation of NM protein.....	16
4.3.1	Ni-IMAC Chromatography	16
4.3.2	Fibrillization of recombinant NM protein	17
4.4	Cell biological methods.....	17
4.4.1	Cryoconservation and thawing of cells	17
4.4.2	Cultivation and passaging of N2a cells	18
4.4.3	Determination of cell number	18
4.5	Quantification of intracellular aggregates prior to fibril exposure.....	18
4.5.1	Reverse method	18
4.5.2	Aggregate induction assay	19
4.5.3	Determination of optimal cell seeding number and time for aggregate induction assay	19
4.5.4	Nuclei staining and automated confocal microscopy.....	19
4.5.5	Image and statistical analysis	20
4.5.6	Statistical analysis	20
4.6	Screen	21

4.6.1	Compound preparation (activators and inhibitors of different endocytic pathways)	22
4.6.2	Compound spotting using the Echo 550 system	22
4.7	Chemicals	24
4.8	Consumables	24
4.9	Cell Culture Medium and Supplements	25
4.10	Instruments and Accessories	25
4.11	Microscopes	26
4.12	Software	26
4.13	Other used material	26
5	RESULTS	27
5.1	Establishment of a cell-based aggregate induction assay for a high content screen..	27
5.1.1	Sonication of the NM fibrils increases the aggregate induction rate in the NM-GFP cells	27
5.1.2	Chloroquine diphosphate salt is a prominent aggregate induction activator .	29
5.1.3	NM seeds produced by rotation at 4°C exhibit a higher aggregate induction activity than fibrils produced at room temperature	31
5.1.4	Reverse method with pre-adsorbed fibrils decreases induction efficiency	32
5.1.5	Higher N2a NM-GFP cell passage number has no significant effect on the aggregate induction	32
5.1.6	Optimised cell pre-seeding and fibril incubation time in the aggregate induction assay	33
5.2	Screen with endocytic inhibitors reveals that macropinocytosis is involved in NM aggregate induction.....	35
5.2.1	Latrunculin A, cytochalasin A and cytochalasin D reduce the aggregate induction rate.....	36
5.2.2	Dynamamin inhibitors slightly increase the aggregate induction rate	39
5.2.3	Specific clathrin or caveolae inhibitors show no effect on the aggregate induction.....	41
5.2.4	Inhibition of macropinocytosis decreases the number of cells with induced NM-GFP protein aggregates	42

6	DISCUSSION.....	46
6.1	The yeast Sup35NM domain is suitable for the cell-based aggregate induction assay	46
6.1.1	Optimised NM fibril aggregate induction assay for high content screening..	47
6.1.2	NM fibril preparation	47
6.1.3	NM-GFP protein aggregate induction.....	49
6.2	The screen revealed interesting endocytic pathways involved in NM fibril aggregate induction	49
6.2.1	Actin disruption reduces aggregate induction.....	50
6.2.2	Macropinocytosis is involved in aggregate induction.....	51
6.2.3	Dynamin inhibition may up-regulate macropinocytosis	53
6.2.4	Genistein affects the morphology of the induced NM-GFP protein aggregates	53
6.3	Relevance of this study	54
7	CONCLUSION.	55
8	REFERENCES	57

LIST OF FIGURES

Figure 1: Schematic diagram of the PrP structural features	3
Figure 2: Molecular mechanism of the fibril formation	4
Figure 3: Schematic representation of Sup35 domains	7
Figure 4: Prion life cycle	9
Figure 5: Major endocytic pathways	12
Figure 6: Work flow for screening	21
Figure 7: Sonication of fibrils increases the endogenous aggregate induction rate	28
Figure 8: Impact of the compounds on the NM-GFP protein aggregate induction.....	29
Figure 9: Chloroquine diphosphate salt increased the percentage NM-GFP ^{agg} cells	30
Figure 10: Fibrils rotated at 4°C display a higher aggregate induction activity.....	31
Figure 11: Reverse method induced less aggregates than the standard method.....	32
Figure 12: Higher passage does not influence the aggregation rate in NM-GFP cells.	33
Figure 13: Optimal cell seeding time prior to fibril application and fibril incubation time	34
Figure 14: DMSO controls	36
Figure 15: Latunculin A, cytochalasin A and cytochalasin D treated cells.....	37
Figure 16: Dose response curves for latrunculin A, cytochalasin A and cytochalasin D....	38
Figure 17: Dose response curves for dynamin inhibitors.	39
Figure 18: Cells treated with dynamin inhibitors	40
Figure 19: Dose response curves for clathrin and caveolae inhibitors	41
Figure 20: Dose response curves for macropinocytosis inhibitors.....	43
Figure 21: Cells treated with FRAX486 and EIPA	44
Figure 22: Cells treated with genistein	45

LIST OF TABLES

Table I: Endocytosis activators and inhibitors	22
--	----

LIST OF ABBRAVIATIONS

Å	ångström
aa	amino acid
ADP	adenosine diphosphate
agg	aggregation
Asn	asparagine
AFM	atomic force microscopy
BSE	bovine spongiform encephalopathy
CJD	Creutzfeldt-Jakob disease
CM	cold medium
CQ	chloroquine diphosphate salt
C-terminal	carboxyl terminal
DMSO	dimethyl sulfoxide
DNA	deoxyribonucleic acid
E. coli	escherichia coli
EDTA	ethylenediaminetetraacetic acid
EGF	epidermal growth factor
FFI	fatal familial insomnia
GFP	green fluorescent protein
Gln	glutamine
GPI	glycosylphosphatidylinositol
GSS	Gerstmann–Sträussler–Scheinker syndrome
HA	hemagglutinin
Hsp	heat shock protein
LB	lysogeny broth
NHE	Na ⁺ /H ⁺ exchanger

N-terminal	amino terminal
OPR	oligopeptide repeats
p	probability of obtaining the observed sample results
PAK	p21-activated kinase
PBS	phosphate buffered saline
PFA	paraformaldehyde
PI3K	phosphoinositide 3-kinase
PMCA	protein misfolding cyclic amplification
PrP ^C	cellular prion protein
PSPr	protease-sensitive prionopathy
PrP ^{Sc}	abnormal form of prion protein
RFP	red fluorescent protein
rpm	rounds per minute
SDS	Sodium dodecyl sulfate
SEM	standard error of the mean
siRNA	Small interfering ribonucleic acid
SOD-1	Superoxide dismutase-1
sol	soluble
ThT	thioflavin T
TK	tyrosine kinase
TSE	transmissible spongiform encephalopathies
WM	warm medium

POVZETEK

Prenosljive spongiozne encefalopatije so nevrodegenerativne bolezni osrednjega živčevja, ki jih povzročajo prioni zaradi njihovega neprimerne zvitja in kopičenja njihovih agregatov. Strokovni termin prion se je prvič pojavil leta 1982, ko je Nobelov nagrajenec Stanley Prusiner odkril delec, odgovoren za bolezen praskavko pri ovcah in ga poimenoval »proteinski prenosljivi delec«. Praskavka pri ovcah je bila tudi prva opisna prionska bolezen, za katero je odgovoren celični prionski protein (PrP^{C}), ki se ob stiku z nenormalno obliko, poimenovano PrP^{Sc} ¹, preklopi v rastoči se agregatni delec, bogat z β -strukturami. Prionske bolezni, ki so jih odkrili pri človeku in drugih sesalcih, so izjemno redke, neozdravljive in smrtne bolezni. Najpogostejša oblika je Creutzfeldt-Jakobova bolezen, ki se pojavi pri eni osebi na milijon prebivalcev. V skupino prionskih bolezni pri človeku uvrščamo še smrtonosno družinsko nespečnost in Gerstmann-Sträussler-Scheinkerjev sindrom, ki sta odraz mutacije na genu za PrP^{C} , kuru, bolezen ljudožerskih plemen na Papui Novi Gvineji in nedavno identificirano proteaze-senzitivno prionopatijo. Zanimanje za prionske bolezni se je izjemno povečalo v 90. letih prejšnjega stoletja, ko so v Veliki Britaniji zaznali novo obliko Creutzfeldt-Jakobove bolezni, nastale zaradi uživanja okuženega govejega mesa.

Raziskovanje teh bolezni so znatno pospešili uveljavljeni modeli celičnih kultur, ki so izboljšali razumevanje delovanje mehanizmov prionov. *Ex vivo* se agregati prav tako tvorijo ob stiku nenormalne oblike prionskega proteina z normalno fiziološko obliko (PrP^{C}). Točna vloga celičnega prionskega proteina v človeku še ni znana. Zanimivo pa je, da kar nekaj citoplazemskih proteinov v celicah kvasovk deluje na podoben način kot PrP^{C} in so zato bili poimenovani prioni kvasovk. Prioni kvasovk so dokazano izjemno dober študijski model za raziskovanje prionov. Celice kvasovk se namreč izjemno hitro delijo in prioni kvasovk niso smrtonosni delci, ki bi povzročali bolezen, vendar služijo kot epigenetski elementi, ki predrugačijo metabolni fenotip gostitelja. Poleg prionov kvasovk in sesalčjih prionov tudi nekateri drugi proteini tvorijo agregate, bogate z β -strukturo, poimenovane tudi amiloidi. Nedavne študije so pokazale, da se Tau protein, α -synuclein, superoksid dismutaza-1 in nekateri drugi amiloidni proteini znotraj prizadetih organov širijo na enak način kot prioni.

¹ Sc izhaja iz besede Scrapie, kakor je poimenovana praskavka v angleškem jeziku

Da bi razumeli delovanje prionov in drugih proteinov s podobnimi lastnostmi, se moramo najprej poglobiti v mehanizme, ki so odgovorni za njihovo prenosljivo naravo in sposobnost agregacije identičnih proteinov. To vključuje tudi razumevanje vstopa prionov in proteinskih agregatov v celico. V tej magistrski nalogi smo skušali pojasniti vlogo endocitotskih poti pri tvorbi agregatov citosolnih prionov. V ta namen smo uporabljali nevroblastne celice mišje celične linije (N2a), ki so izražale prionsko NM domeno Sup35 proteina (Sup35NM) iz kvasovk, sklopljeno z zelenim fluorescenčnim proteinom (green fluorescent protein; GFP). Kot že omenjeno, sesalčki prioni pri človeku povzročajo neozdravljive simptome in so izjemno nevarni. Na drugi strani prioni iz kvasovk delujejo na zelo podoben način in niso nevarni človeku.

Sup35 je po svoji funkciji citosolni translacijski dejavnik, ki se pod določenimi pogoji prestrukturira in agregira. Agregacijo predhodno topnega Sup35NM smo v NM-GFP celicah izzvali z izvenceličnimi *in vitro* proizvedenimi fibrilnimi vlakenci istoimenskega proteina. Namena tega projekta sta bila: a) optimizacija celične metode, primerne za visokozmogljive analize, ki vključujejo avtomatizirano konfokalno mikroskopijo z obširno statistično obdelavo izbranih parametrov in b) uporaba te metode za študij vpliva endocitotskih poti na tvorbo agregatov, ki vključuje znane kemične zaviralce določenih endocitotskih poti. V predhodnih študijah je že bilo dokazano, da NM domena Sup35 proteina predstavlja ustrezen model za študije splošnih vidikov vstopa izvenceličnih agregatov, ki so zmožni izzvati agregacijo citosolno izraženih prionskih proteinov. Sesalčje celice namreč ne vsebujejo homologne sekvence NM domene, zato je vstop le te ni odvisen od fiziološke receptorske endocitoze. Poleg tega rekombinantna NM vlakenca učinkovito izzovejo agregacijo ektopično izraženega identičnega proteina. In še, proteini iz kvasovk ne delujejo citotoksično na sesalčje celice. Te študije so dokazale tudi, da prionska domena Sup35NM v sesalčjih celicah izpolnjuje vse pogoje reprodukcijskega cikla prionov: (I) prekursorski protein je prisoten v topni obliki, (II) tvorba agregatov je lahko izzvana s strani zunajceličnih vlakenc identičnega proteina, (III) izzvani prionski agregati so mitotsko stabilni, (IV) prionski agregati se lahko razširijo na sosednje celice, kjer izzovejo samo-ohranjevalno prionsko stanje ob prisotnosti prekursorskega proteina.

Za študij vloge endocitotskih poti pri tvorbi agregatov smo najprej razvili stabilno metodo z visoko ponovljivostjo rezultatov, ki ponuja dovolj visoko število celic z agregati. V nadaljevanju smo določili parametre, ki so bili potrebni za analizo slik, pridobljenih s

konfokalno mikroskopijo. Z optimizacijo metode smo omogočili nadaljnje raziskave, kjer smo uporabili endocitotske inhibitorje in določali število celic, ki vsebujejo agregate. Pri tem smo vrednotili tudi citotoksičnost izbranih zaviralcev.

Prvotno smo v celičnem modelu lahko izvali le 5% stopnjo agregacije. V postopku optimizacije smo optimirali sledeče parametre: število celičnih pasaž, začetno število celic za zasejanje, rotacijsko koncentracijo in temperaturo rotacije NM domene, obdelavo NM vlakenc z ultrazvokom in končno koncentracijo NM vlakenc. Testirali smo tudi nekaj možnih spodbujevalcev endocitoze in različnih gojišč za razredčevanje NM vlakenc pred nanosom na celice. Hkrati smo preizkusili tudi različne postopke, ki so vključevali vrtenje plošč med inkubacijo ali predhoden nanos vlakenc na dno testnih plošč. Po končani optimizaciji metode smo lahko izvali 50% stopnjo agregacije, kar potrjuje, da je bila optimizacija uspešna. Visokozmogljive analize z uporabo konfokalne mikroskopije so razkrile nekaj endocitotskih mehanizmov, ki vplivajo na stopnjo agregacije v NM-GFP celicah. Na stopnjo agregacije niso vplivali zaviralci klatrinskih in kaveolskih poti. Smo pa zato zaznali močen upad stopnje agregacije pri uporabi zaviralcev, ki delujejo na različne mehanizme, povezane z makropinocitozo. Kemični zaviralci kot so EIPA, FRAX486 in wortmannin so drastično znižali odstotek celic, ki so vsebovale agregate in s tem nakazali, da je tvorba agregatov citosolnih proteinov odvisna od te vrste vstopne poti. Ti zaviralci so se izkazali za najprimernejše kemične spojine, saj v uporabljenih koncentracijah sočasno z zaviralnim učinkom na agregacijo niso izkazali toksičnih učinkov. Vsekakor moramo hipotezo, da so NM vlakenca res vstopila v celico preko makropinocitoze, še potrditi. Najprej moramo s fluorescenčno označenimi kazalci potrditi, da so kemični zaviralci res delovali na omenjeno vstopno pot. V ta namen bomo uporabili komercialno dostopne fluorescenčno označene kazalce za določeno vrsto endocitoze. Fluorescenčno označene kazalce bi uporabili tudi za ugotavljanje kolokalizacije z označenimi NM vlakenci v citoplazmi. V nadaljevanju bi sledili tudi njihovem vstopu v celice. Pri tem bi celice transficirali z LifeAct plazmidom, s čimer bi lahko opazovali dinamiko aktinskih vlaken v realnem času med vstopom NM vlakenc v celice.

Predhodne študije so pokazale, da podobno kot prioni iz kvasovk tudi sesalčki prioni in drugi proteini, udeleženi v nevrodegenerativnih boleznih, kot so superoksid dizmutaza-1, Tau protein in α -synuclein vstopijo v celice preko makropinocitoze. To še dodatno potrjuje hipotezo, da imajo ti proteini nekatere skupne lastnosti.

ABSTRACT

Prion proteins in a misfolded aggregated state are responsible for transmissible spongiform encephalopathies, fatal neurodegenerative disorders. More and more evidence accumulates that prion-like cell-to-cell propagation of misfolded proteins is a common mechanism in many neurodegenerative diseases. Prion proteins also exist in fungi, where rather than causing the fatal diseases act as epigenetic regulators. To understand the mechanism of cytosolic protein aggregate uptake, the Sup35^{NM} yeast prion domain tagged with GFP was expressed in mouse neuroblastoma N2a cells. Once endogenous NM-GFP aggregates were induced with exogenous bacterially produced Sup35^{NM} fibrils, they were inherited by daughter cells and were infectious to the neighbouring cells. Aims of this study were to a) establish a cellular assay amenable to high throughput analysis of cytosolic NM aggregate induction, and b) to use this assay to study endocytic pathways involved in the cytosolic prion induction. For this purpose, optimised aggregate induction assay was used to perform two high content screens including different endocytic inhibitors, and monitoring the aggregate induction rate in NM-GFP cells.

Here we show that the aggregate induction rate was not negatively affected by clathrin- or caveolae inhibition, but was strongly reduced upon macropinocytosis inhibition. Our results suggest NM aggregate induction depends on this fluid-phase uptake, since commonly used macropinocytosis inhibitors such as wortmannin, EIPA and FRAX486 drastically decreased the aggregation. Further high throughput analysis including additional macropinocytosis inhibitors will be very important to understand the protein aggregates spreading behaviour.

Our results provide new insights into prion behaviour in mammalian cells, and may help to understand why some cells are more susceptible to aggregate induction. These results could help to explain spreading mechanisms of cytosolic protein aggregates.

Key words: *prion, Sup35, transmission, endocytosis, high content screen*

1 INTRODUCTION

1.1 Prions – the infectious agents

Prion proteins in their misfolded aggregated state are responsible for a class of fatal neurodegenerative diseases called transmissible spongiform encephalopathies (TSE). Originally the term prion for “proteinaceous infectious agents” was coined by Stanley Prusiner in 1982. Prusiner introduced the protein-only hypothesis, which states that the cellular prion protein PrP can misfold into the multiple distinct infectious conformations (strains) that cause phenotypically diverse variants of the prion diseases independently of nucleic acid [2, 3]. The prion-only hypothesis is now widely accepted, whereas the early hypotheses suggesting that infectious agent is a slowly progressing virus [4] or includes genome coding sequences were rejected [5]. Prion strains are the conformational isoforms of the abnormal protein that are distinct in structure and lead to different incubation times. The protein-only hypothesis states that each strain is associated with its own abnormal conformer, which is compatible with the different patterns of proteolysis and glycosylation of PrP [6]. It has been proposed that the strain properties are enciphered in the tertiary structure of the pathological form. [7].

Scrapie disease in sheep is the first described prion disease, where the cellular prion protein (PrP^{C}) is converted into its abnormal form (PrP^{Sc}), causing a severe brain damage. The abnormal form was later shown to be the main component of the infectious agent, therefore the pathological form PrP^{Sc} (for Scrapie) was named after this disease [8, 9]. Since then prion diseases were subcategorized into genetic, sporadic or idiopathic forms, all of which involve conformational changes of PrP^{C} into the PrP^{Sc} and affect humans and other mammals. Additionally, it was determined that prion diseases are infectious and can be transmitted experimentally or in nature within or between species [10]. Following exposure to the pathogenic PrP^{Sc} , PrP^{C} changes from a soluble into a less soluble aggregated pathologic form, which accumulates mainly in the central nervous system but also in lymph nodes, tonsils, and Peyer’s patches of the digestion tract [11]. Remarkably it could also be found in the removed appendix, even before the clinical symptoms [12].

Human prion diseases are considerably rare, incurable and fatal diseases. The most frequent form, the sporadic Creutzfeldt-Jakob disease (CJD) occurs in about one per million people annually, typically without clear evidence of the exposure to the infectious

agent [13]. Besides CJD, human prion diseases include fatal familial insomnia (FFI), Gerstmann-Sträussler-Scheinker syndrome (GSS) and the recently described protease-sensitive prionopathy (PSPr) [14], both mostly occur sporadically and kuru, which originates from dietary infection [4]. Several mutations in the *Prnp* gene located on the chromosome 20 also cause genetic human prion diseases. More than 30 mutations in the *Prnp* gene are connected to the inherited human prion diseases, including familiar CJD, FFI and GSS [2]. Familiar TSE in humans are extremely rare and were identified only in few families worldwide.

To date, the most studied prion disease in animals is scrapie affecting sheep and goats [3]. The scrapie agent causes spongiform changes in the brain as well as neuronal loss, astrogliosis and microgliosis [3, 15]. Bovine spongiform encephalopathy (BSE) in cattle, often referred to as mad cow disease, is also one of the most examined disorders [16]. Other described animal prion diseases are chronic wasting disease in deer, elk and moose, and transmissible mink encephalopathy in captive mink [17, 18]. In animals, no naturally occurring genetic prion diseases were yet identified. It appears that lack of the infectious agent in excreta restricts horizontal transmission within the species in some prion diseases [19]. Transmission between animals via milk, saliva or urine was observed in moose [19]. Furthermore, BSE agent is highly infectious via oral route in cattle [2]. In humans, some cases of blood transfusion-related transmission of CJD have been observed [15]. Since PrP^{Sc} has been found to be resistant to high temperature, high pressure, formaldehyde and ultraviolet radiation, iatrogenic transmission has happened [15]. Prion diseases were also transmitted during neurosurgery or during growth hormone therapy [2]. Furthermore, an outstanding number of cases of transmission from human to human resulted from a ritual cannibalism reported in the Fore people of Eastern Highlands in Papua New Guinea [4]. The disease was transmitted during oral consumption of kuru-infected organs.

1.2 Biochemical characteristics of prions

Human cellular prion protein PrP^C is a 254 amino acid long protein, with a signal peptide and a 22 amino acid signal peptide for glycosylphosphatidylinositol (GPI) anchor attachment to the C-terminal. It has a globular domain with three α -chains and two short anti-parallel β -strands and it is adhered to the outer cell membrane by the GPI anchor [8].

While TSE-specific PrP^{Sc} is infectious and causes neuronal death, PrP^C in its native form is neuroprotective [8]. Location on the cell membrane suggests that PrP^C is involved in cell adhesion and molecular signalling [20]. However, the exact cellular function remains to be clarified. In contrast to the predominantly α -helical carbonyl-terminal (C-terminal) domain of the PrP^C, PrP^{Sc} is enriched in β -structure. PrP^C holds 47% α -helix and 3% β -structures, whereas PrP^{Sc} contains approximately 17-30% α -helix and 43-45% extended β -structures [21]. PrP^{Sc} is partially resistant to hydrolysis by the proteinase K and insoluble in detergents such as SDS. By contrast, PrP^C is completely soluble in detergents and fully digested by the aforementioned proteinase [8]. These characteristics are used in biochemical assays to discriminate between normal and pathological forms of the prion protein. Due to insoluble nature of the PrP^{Sc}, no defined structure has yet been determined. Several models have been proposed for the PrP^{Sc} structure. In one model, left-handed β -helixes have been proposed as the most likely substructures for the PrP^{Sc} [22]. Prion proteins form amyloid structured fibrils, which are 40-120 Å long, straight, unbranched filaments. Electron microscopy revealed that the typical amyloid fibril normally consists of 2-6 protofilaments, twisted together to form a 7 to 13 nm wide rope [23]. Within the fibrils, β -sheets run perpendicular to the fibril axis, the strands aligned via hydrogen bonds between carbonyl groups and amides of the polypeptide chain. Highly charged residues and hydrophobicity most probably favour protein aggregation [23]. The highly ordered amyloid structures have enhanced affinity for certain dyes. Both thioflavin T (ThT) and Congo red bind to the β -structures in the fibril [24, 25].

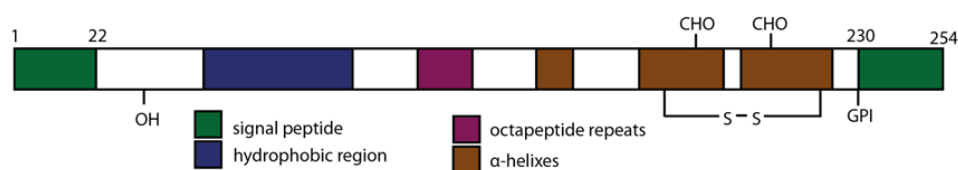


Figure 1: Schematic diagram of the PrP structural features including N- and C-terminal signal peptides, metal ion-binding octapeptide region, single disulfide bridge and the GPI anchor. Numbering is according to the murine protein.

Prions replicate by a mechanism of seeded-polymerization. This is a relatively slow process of the initial seed formation [26]. Seeds later serve as the templates to promote homotypic protein monomers in their native structure to misfold and become incorporated into the amyloid structured fibril (Figure 2) [27, 28]. Several conditions can promote the fibril formation: Increased concentration of the respective aggregation-prone protein; mutations that destabilize the native form, and allow interaction of amyloid segments to interact with each other; exposure to pre-formed amyloid seed of same protein; and thermodynamically destabilizing conditions such as pH or temperature. Furthermore, *in vivo*, impaired cellular proteostasis also stimulates the process [29].

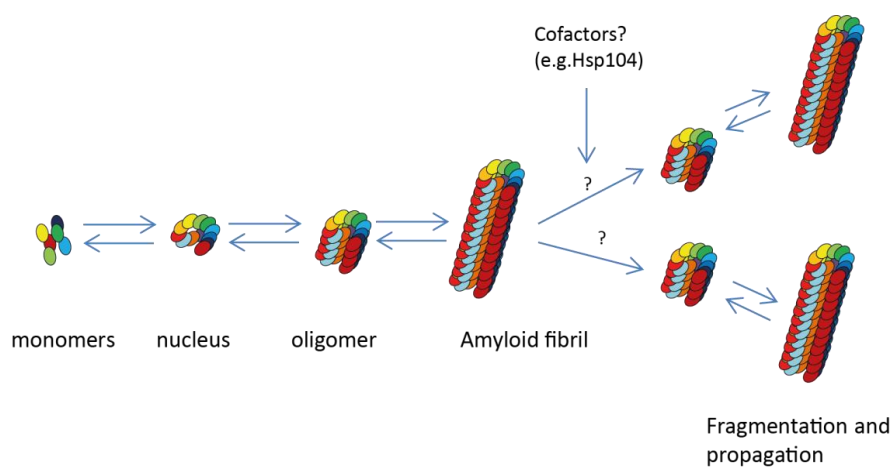


Figure 2: Molecular mechanism of the fibril formation. When conditions are fulfilled, the process of nucleation is set in motion. A lag phase is required to form a nucleus. During the elongation phase, oligomers and/or monomers are incorporated into growing fibrils. Fibril fragmentation generates seeds that serve later as new templates for fibril formation.

Subsequently, secondary nucleation events were proposed to accelerate the aggregate formation. Here, fragmentation of the existing fibrils generates new seeds for further recruitment and conversion of homotypic proteins, which are capable to misfold [27, 28]. Soto and colleagues verified this theory by developing a protein misfolding cyclic amplification assay (PMCA), a technique to produce infectious prion seeds *in vitro* [30]. In this system, a small amount of PrP^{Sc} and a surplus of the PrP^C units are mixed. During repeated cycles of incubation and sonication, new fibrils are being generated and fragmented into the new potential seeds. As a result of this amplification, infectious PrP^{Sc} seeds were generated *in vitro*, which reinforced the protein-only hypothesis.

1.3 Prions can propagate in cell culture

Established prion cell culture models have indeed improved the understanding of cellular prion mechanisms. *In vitro* prion replication and propagation starts with the PrP^{Sc} infection. Infective agents are first attached to the cell membrane, from where they are taken up [10]. This was reported to be neither cell type nor strain dependent [31]. As normal cellular prion protein is attached to the outer membrane via GPI anchor, conversion to its pathological form is believed to occur either on the cell surface or along the early endocytic pathway [10]. This suggests that PrP^C protein might serve as a receptor for its PrP^{Sc} to enter the cell [31]. Moreover, some studies exposed lipid rafts as important component for PrP^{Sc} formation and uptake [10, 31]. Although several receptors and endocytic pathways have been proposed to take part in this process, mechanisms of uptake remain unclear. Upon internalization, PrP^{Sc} is mostly found in vesicles including early endosomes, recycling endosomes, and lysosomes [10]. Substantial amount of the newly formed PrP^{Sc} are already detectable within minutes, indicating that conversion from PrP^C to PrP^{Sc} is extremely fast process [10, 31]. Interestingly, in some cell lines over-expression of the PrP^C did not affect the initial binding of the PrP^{Sc}, suggesting that amount of the PrP^C is insignificant for the uptake [10, 31].

Mammalian prions can be successfully replicated in most cell culture models [31]. However, for the continuous prion propagation in the cell culture, larger infectious entities must be fragmented into smaller seeds. To do so, it is possible that large aggregates are splintered by mechanical force [10]. Alternatively, undefined cofactors in the vesicle compartments might be involved [10]. Productive infection in the cell culture has been shown with the persistent presence of the abnormal form over multiple passages [31]. Here, the prion phenotype is faithfully inherited by the daughter cells and prions can invade neighbouring cells [10, 22]. Thus, at least two independent routes are involved in prion transmission *in vitro*: horizontal transmission to the bystander cells or vertical transmission to the daughter cells [10]. Importantly, transmission to the bystander cells can again spread horizontally or vertically to the daughter cells [10]. However, not only mammalian prions, but also prions in lower eukaryotes like yeast can horizontally and vertically propagate in the cell culture models.

1.4 Yeast prions

Several cytoplasmic proteins of yeast and filamentous fungi also share the self-perpetuating and propagation characteristics of mammalian prions and were thus termed yeast prions [32]. Reed Wickner postulated criteria for prions in these lower eukaryotes [32]. First, prion phenotype is reversibly curable, meaning prion form can arise again from the cured yeast. Second, overproduction of a protein increases the chance of spontaneous prion induction, simply because of higher probability for the potential misfold. Third, the genetic code for the normal protein form is essential, since prion phenotype can only propagate by converting the normal form into the prion form [32]. Additionally, despite the fact that yeast prions differ in localisation from mammalian prions, both types have shown notable similarities in their life cycle [10].

A few proteins in yeast have been identified that can misfold into aggregated prion states, such as Ure2, Sup35, Rnq1 and New1 [1]. Yeast prions have been proven to be a great model system to study prion life cycle in detail. First, yeast cells have a fast growth rate and second, the yeast prions are not fatal agents but rather serve as epigenetic elements of inheritance that alter the metabolic phenotype of the host [33]. In its soluble, non-prion form, Ure2 is a transcriptional activator, while the Sup35 functions as cytosolic translation termination factor [1]. The aggregation of Ure2 and Sup35 leads to the prion [*URE3*] and [*PSI+*] phenotypes, respectively, that impair the normal activity of the proteins [1, 32]. Importantly, all previously mentioned yeast prions are in contrast to mammalian prions cytosolic.

Sup35 as one of the best studied yeast prions consists of 685 amino acids. It is composed of the N-terminal domain (aa 1-123), which is required for prion maintenance [34, 35]. The highly charged middle region (aa 124-253) is necessary for mitotic prion stability and increases its solubility in the non-prion state of the protein [36]. The C-terminal domain (aa 254-685) is essential for its translation termination function but not for prion formation [34, 37]. Since the NM (Sup35NM) domain alone can be expressed in yeast and can adopt a heritable prion conformation, it is often used in prion studies [34]. Interestingly, similar to PrP^{Sc}, also the aggregates of Sup35NM were found to be partially proteinase-K resistant [25]. The N domain with prion forming properties is further comprising a glutamine (Gln) and asparagine (Asn) rich region followed by five and a half oligopeptide repeats (OPR)

(Figure 3). The Gln/Asn rich region contains a high content of polar and unchained amino acids [38] and was suggested to be involved in the intermolecular interactions between the Sup35 monomers. Initially, however, a rare event of oligomer formation has to occur, which reorganises the conformation of the protein into an ordered aggregated state [39]. Generation of such a seed occurs spontaneously at low frequency ($1:10^6$) in yeast and leads to the prion phenotype [1]. However, the spontaneous *de novo* prion phenotype can be increased to $1:10^1$ by over-expression of N domain [35].

Soluble Sup35 molecules are believed to exist in a steady state between monomers and oligomers [40]. However, similar to mammalian prions, also yeast prions can form amyloid fibrils [25, 32]. *In vitro*, fibrillization is a two stage process starting with the nuclei formations, which are generated by spontaneous intrinsic conformational rearrangements of monomers and/or oligomers [32]. In second stage, namely fibril formation, seeds recruit soluble Sup35 protein to convert into a growing prion-like aggregate [40]. The prion phenotype in yeast depends on the co-existence of other protein in their prion conformations, namely RNQ1 [35]. Since fibril formation and replication are required for prion propagation, many cellular factors have been shown to play an important role in this process. Heat shock protein 104 (Hsp104) in conjunction with other components of the chaperone family acts as a disaggregase that disassembles prion aggregates [41]. It seems to be essential for efficient prion transmission to daughter cells, since it breaks the big aggregates into smaller transmissible units [10]. The disaggregase Hsp104, which seems to be responsible for the fragmentation in yeast, does not exist in mammalian cells [10].

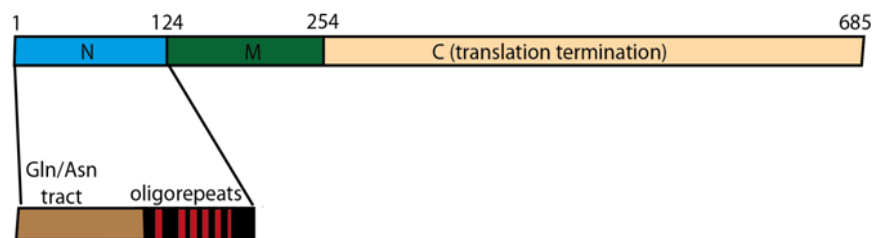


Figure 3: Schematic representation of Sup35 domains. N-terminal domain rich in asparagines (Asn) and glutamines (Gln) flanked C-terminally by oligopeptide repeats is necessary for prion formation. The highly charged middle domain influences the prion stability during mitosis and the C-terminal domain fulfils the translation termination function. Adapted from [1]

1.5 The Sup35 model system in mammalian cells

The yeast prion Sup35 is a cytosolic protein, which provides us with a good model to understand the properties of the cytosolic prion proteins. It has already been shown that the recombinant Sup35NM domain under certain conditions forms fibrils, which can induce the prion phenotype in yeast [42]. Since all the studies of Sup35 are performed in yeast, Krammer and colleagues in our group have previously generated a suitable cell culture model including the yeast Sup35NM domain and N2a (mouse neuroblastoma) cells [43]. To study whether cytosolic protein aggregates in mammalian cells can also behave as infectious entities that can transmit vertically to daughter cells and horizontally to bystander cells [43], the prion phenotype was induced using *in vitro*-generated NM fibrils. To this end, N2a (mouse neuroblastoma) cells were transduced with lentivirus coding for the hemagglutinin antibody epitope tagged (HA-tagged) Sup35NM domain [43]. Additionally, recombinant NM fibrils were generated by rotation of monomeric Sup35NM domain. Successfully produced fibrils were confirmed by atomic force analysis and applied to the N2a cells expressing soluble protein (NM-HA^{sol}). NM-HA protein remained soluble in cells not exposed to the fibrils (NM-HA^{sol}) [43]. Contrary, in about 50% of NM-HA^{sol} cells exposed to the NM fibrils, aggregation of the NM-HA was induced (NM-HA^{agg}). Additionally, total NM (exogenous and endogenous) was detected using NM-specific antibody 4A5 and anti-HA antibody within the cytosol [43]. Interestingly, some NM fibrils were found in the cells that did not co-stain with the anti-HA antibody. This indicated that cytosolic aggregation of the endogenous NM-HA was induced by the uptake of exogenous fibrils [43].

The percent of cells with aggregates did not decrease after one passage after exposure and was still evident after ten passages, showing that aggregated state was inherited by daughter cells [43]. Interestingly, NM fibrils induced several morphologically diverse aggregate types, which were observed in close proximity [43, 44]. That could be explained by the fact that distinct NM-HA aggregates were induced by diverse NM variants/strains and were further inherited by daughter cells or propagated to neighbouring cells [44]. Parallel to NM-HA^{sol} cells, N2a cells expressing a green fluorescent protein tagged (GFP-tagged) Sup35NM domain (NM-GFP^{sol}) were produced in the same way with lentivirus to study intercellular aggregate transmission [44]. When both cell types NM-HA^{agg} and NM-GFP^{sol} were mixed and incubated as a coculture for several hours, NM-GFP cells with

induced NM-GFP aggregates (NM-GFP^{agg} cells) were observed [44]. In some instances, NM-HA aggregates were also visible in recipient NM-GFP cells, indicating that aggregates were transmitted from donor to recipient cells [44]. This indicates that not only NM fibrils, but also NM-HA aggregates in a coculture system are infectious to the neighbouring cells as prions [43, 44].

So far, Krammer et al. and Hofmann et al. could successfully demonstrate that the ectopically expressed yeast prion domain Sup35^{NM} fulfils all criteria of the prion life cycle in mammalian cells [43, 44]. This model system also proved that Sup35^{NM} fulfils all cellular replication criteria of mammalian prions: the precursor protein is present in a soluble non-prion state; prion formation can be initiated by exogenous seeds; induced prion aggregates are mitotically stable; and prions can spread to neighbouring cells in which they induce a self-perpetuating prion state of the substrate protein [44]. This proved that our model system is appropriate to study cytosolic prion formation in mammalian cells.

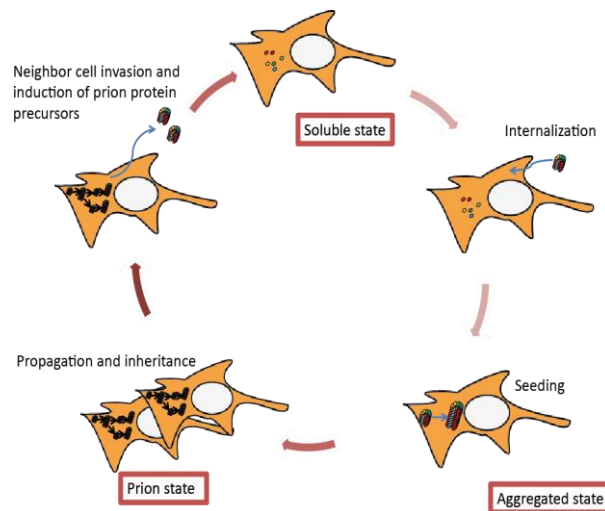


Figure 4: Prion life cycle. Cells with soluble prion proteins can be induced by exogenous homotypic fibrils to aggregate. Induced aggregates successfully propagate and are stably inherited during mitosis. Prion entities naturally invade neighboring cells and induce a self-perpetuating state.

The mechanism of fibril uptake from the medium or the exact mechanisms of cell-to-cell transmission remain unclear. Condition medium from cell cultures including NM-HA^{agg} cells was found to be less effective in aggregate induction of recipient cells, suggesting that secretion of NM-HA^{agg} in the coculture system is not the main pathway for aggregate transmission [44]. In the coculture system, direct cell contact appears to be required for aggregate induction. NM aggregates could be transmitted via filopodial bridges or

nanotube-like structures as observed for some viruses [44]. It is also possible that aggregates are released into the intracellular cleft to be taken up by the neighbouring cells [44]. In cell culture mammalian prions have been shown to use exosomes, direct cell contact or tunnelling nanotubes to exit the cell and enter the neighbouring cell [44]. The uptake of PrP^{Sc} when added to the medium appears to depend on macropinocytosis [45]. Similar to mammalian prions, also some prion-like aggregates such as mutant superoxide dismutase-1 (SOD-1) aggregates have been proposed to use macropinocytosis to enter the cell [46]. So far it is unclear how fibrils formed from recombinant Sup35NM are taken up by the cell and induce aggregation of the NM expressed in the cytosol but it is possible that endocytic pathways play a role.

1.6 Endocytic pathways

Many pathogens utilize cellular pathways for cell entry [47]. Also mammalian prions invade their target cell to implement productive infections, but the precise mechanism of uptake is unclear. Endocytosis is a major process for the cell to absorb extracellular nutrients and is critical for intracellular signalling and membrane recycling [47, 48]. By distinct energy-consuming endocytic pathways, cells mostly take up large polar molecules, which are unable to cross the lipid bilayer. For each of them the formation of budding structures is essential. Since clathrin coated-pits are clearly visible by electron microscopy it is easy to distinguish between clathrin-dependent and –independent endocytosis. The most common non-clathrin pathway is the caveolae-dependent pathway. The third major endocytic pathway, macropinocytosis, occurs in highly ruffled regions forming actin extensions around extracellular fluid [48].

Clathrin is a triskelion-shaped cytoplasmic protein with three heavy and three light chains [48]. Clathrin-dependent pathway is implicated in the internalization of extracellular ligands, bacterial toxins, certain viruses, and recycling of GPI-anchored proteins [48]. Binding of the cargo to some cell membrane receptors promotes the clathrin-dependent pathway, which is mediated by a group of adaptor and accessory proteins [47]. According to current models they coordinate clathrin nucleation and clathrin-pit formation around the newly formed vesicle. This process leads to well-defined morphological structures that subsequently undergo invagination before scission. After the deeply invaginated vesicle

enclosed by clathrin-coated pit is formed, the neck narrows and the vesicle are subsequently pinched off from the plasma membrane by the large GTPase - dynamin [47]. Several studies suggest that dynamin plays similar role also in the caveolae-dependent pathway. Caveolae are flask-shaped buds existing in the lipid raft area of the mammalian cells. Multicaveolar assemblies, with many connected caveolae are commonly observed. Caveolae budding is regulated by phosphatases and kinases [49] and requires cholesterol-binding protein caveolin and glycolipids. Membrane invaginations formed by this process occur in lipid rafts, organised microdomains containing glycosphingolipids and protein receptors [48].

Macropinocytosis is an efficient pathway of cellular uptake, where invaginations engulf extracellular fluid and macromolecules into the large vesicles. It is either constitutive or stimulated by growth factors such as epidermal growth factor (EGF) or platelet-derived growth factor [48, 50]. A number of proteins have been implicated in controlling this process, including actin [51], Rho family of GTPases (Rac and Cdc42) [51, 52], p21-activated kinases (PAK), tyrosine kinases, phosphoinositide 3-kinase (PI3K), ADP-ribosylation factor-6, and others [47]. There is also evidence suggesting that macropinocytosis is cholesterol dependent, since cholesterol is required for recruitment of the activated Rac GTPases to the site of action [47].

To study the mechanisms of different endocytic pathways, different compounds that target specific components in distinct pathways have been identified and are widely used. Compounds like pitstop1 and pitstop2, inhibitors of clathrin assembly are often used to study clathrin-dependent pathway [53]. Due to dynamin's major role in membrane scission after vesicle formation, it is considered a prominent target to inhibit clathrin- and caveolae-dependent pathways [48, 54]. Since macropinocytosis involves the formation of actin coated vesicles, actin inhibitors have been used as specific inhibitors of this pathway [54]. Besides, macropinocytosis uptake could be blocked specifically by inhibiting PAKs, which belong to a family of serine/threonine kinases [50]. Previous studies indicated their involvement in cytoskeletal dynamics, including membrane ruffling and organization of lamellipodia. PAKs are targets of small GTP binding proteins like Rac1 and Cdc42. Na^+/H^+ antiporter is also often used as the target to study macropinocytosis [55]. The PI3K activity is as well important for the uptake and its inhibitors have been shown to block macropinocytosis.

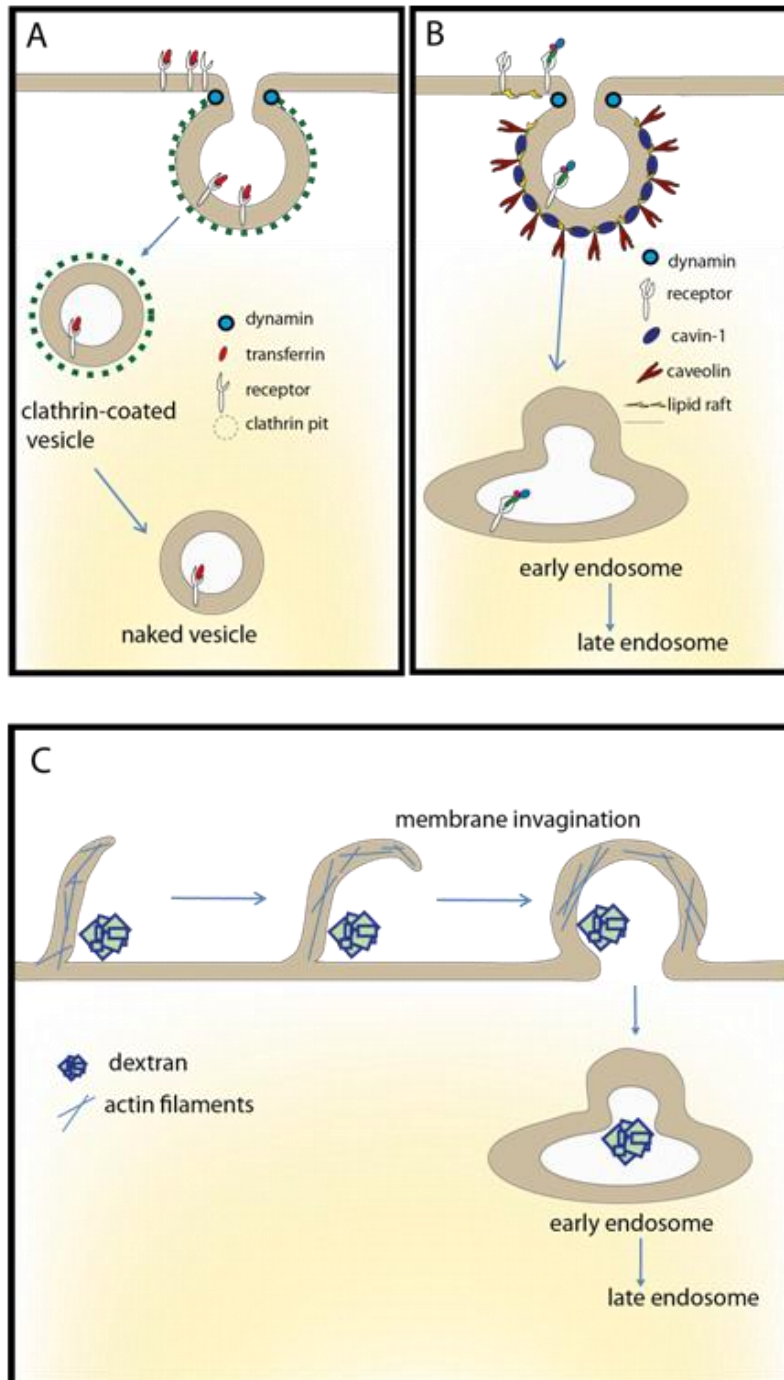


Figure 5: Major endocytic pathways. (A) Clathrin-dependent endocytosis is triggered by binding of the ligand to the cell receptor. Adaptor proteins concentrate around the receptor tail and promote the clathrin polymerization around the newly formed invagination. Subsequently, the vesicle is enclosed with the clathrin-coated pit and pinched off from the membrane by dynamin. The internalized vesicle is uncaged and delivered to the early endosomes. **(B)** Endocytosis via caveolae typically occurs in lipid raft areas, forming 50-70 nm wide flask-shaped invaginations. Adaptor molecules such as cavin-1 and caveolin form the structural backbone of the caveolae. Similar to clathrin-dependent endocytosis, the caveolae pathway is receptor-dependent and highly regulated. Vesicles, released from the membrane by dynamin are delivered to the endosomes. **(C)** Macropinocytosis is a dynamin-independent pathway, which occurs as a response to the cell stimulation. Closure of membrane ruffles leads to large macropinosomes, which are delivered to the early endosomes.

2 AIM OF STUDY

To understand the infectious nature of prions and prion-like protein aggregates, more details on the transmission and aggregate induction need to be obtained. This includes the understanding of prion and protein aggregate internalization. In this project, we used mouse neuroblastoma cell line N2a ectopically expressing Sup35^{NM} to study which endocytic route is involved in prion induction by exogenously added preformed NM fibrils. The aim of this project was to a) establish a cellular assay amenable to high throughput analysis of cytosolic NM aggregate induction, and b) to use this assay to study endocytic pathways involved in the cytosolic prion induction. The NM protein represents a suitable model protein to study general aspects of aggregate uptake and cytosolic prion induction by exogenous seeds. First, mammalian proteins share no sequence homology with the NM domain. Thus, NM internalization is not dependent on a known receptor. Second, recombinant NM fibrils efficiently induce aggregation of the ectopically expressed homotypic protein in our model system. Third, yeast prions are not overtly cytotoxic to our cells.

Our previously published data demonstrate that Sup35^{NM} prions in mammalian cells fulfil all replication criteria of the prion life cycle [43, 44]. In our study we will use NM-GFP cells, which will be exposed to exogenous NM fibrils to induce aggregation of the cytosolic soluble NM-GFP protein. To study the involvement of endocytic routes in prion induction, an aggregate induction assay for high content screening will be developed. This requires a stable assay with high reproducibility and preferably high aggregate induction rate. Furthermore, suitable parameters for image analysis need to be determined and implemented in the image processing routine. When the image analysis methods are optimised, the effect of various endocytosis inhibitors on the NM-GFP aggregate induction rate will be tested. Additionally, toxicity of used compounds will be assessed. This study will focus on the fibril internalization with the aim to identify the major endocytic pathway(s) involved in the prion induction.

3 HYPOTHESES

- 1) Sonication and the proper rotation protocol produce NM fibrils with higher aggregate induction efficiency.
- 2) Passage number of recipient N2a NM-GFP cells and NM protein rotation concentration should not affect the fibril induction efficiency.
- 3) Yeast prions are preferably taken up by one of the main endocytic routes.
- 4) When both clathrin and caveolae-dependent endocytic pathways are blocked, macropinocytosis may be up-regulated.
- 5) Most of the cell endocytic inhibitors in higher concentrations may cause cytotoxicity.

4 METHODS AND MATERIAL

METHODS

4.1 Biological Safety

All the work with genetically modified organisms was performed in the S2 laboratory following current laws and guidelines of the German Act on Genetic Engineering. All used materials, buffers, and other biologically contaminated material were collected separately, inactivated and disposed according to official rules.

4.2 Protein biological analysis

4.2.1. Transformation and cultivation of *E. coli* with plasmid DNA

The bacterial expression plasmid pNOTAG-NM was used to produce recombinant NM. Chemocompetent BL21 *E. coli* were carefully mixed with 1-2 µg plasmid DNA on ice for 30 minutes. The bacteria were heat shocked for 45 seconds at 42°C and subsequently cooled on ice for 2 minutes. The bacteria were shaken at 37°C and 750 rpm (Themomixer compact) in 1 ml lysogeny broth (LB) medium for 1 hour. The tubes were centrifuged at 2650 xg for 2 minutes and most of the supernatant was discarded. The bacteria were resuspended in approximately 100 µl supernatant and plated on LB agar plates supplemented with ampicillin (50 µg/ml). The plate was incubated overnight at 37°C. The next morning, the plate was taken out, wrapped with parafilm, and stored at 4°C. In the late afternoon, one colony was selected and inoculated into the 5 ml LB medium. The pre-culture was incubated in a shaking incubator at 100 xg and 37°C overnight. Next morning 5 ml of pre-culture was added to freshly prepared LB media including ampicillin (100µg/ml). The content was distributed into baffled Erlenmeyer flasks up to maximum 25% of the total flask volume. Flasks were set into the shaking incubator at 180 rpm (Shaker LT-X) and 37°C. Samples were taken every two hours to record the reading at OD₆₀₀ using the Nanodrop 2000c. After three hours when the OD₆₀₀ reached 0.6, the protein expression was stopped and the bacterial content was distributed into the centrifuge tubes, which were centrifuged at 2.773 xg for 15 minutes at room temperature. The supernatant was discarded and the pellet was stored at -80°C.

Plasmid

Plasmid pNOTAG-NM for NM expression was designed and purchased from DNA 2.0.

LB Agar (in H₂O dest.)

Bacto Tryptone	10 g/l
Bacto Yeast Extract	5 g/l
NaCl	10 g/l
Bacto Agar	15 g/l
Ampicillin	100 mg/l

4.3 Isolation of NM protein

4.3.1. Ni-IMAC Chromatography

The bacterial pellet was thawed at room temperature and resuspended in 150 ml buffer A1 and incubated for at least 30 minutes at 37°C. Afterwards the suspension was centrifuged at 48380 xg (Avanti J-26XP) for 20 minutes at 25°C to remove insoluble material. The supernatant was loaded to a pre-equilibrated Q-sepharose Fast Flow column and washed with five volumes of buffer A1. The protein was eluted with a gradient of buffer A1 and B1 at a flow rate of 1 ml per minute.

Gradient for Q-sepharose column Time	buffer B1 (%)
0 min	00
30 min	10
90 min	70
105 min	99
120 min	00

Buffer A1 for purification of recombinant NM

Tris, pH 7.2	10mM
Urea	8 M

Buffer B1 for purification of recombinant NM

Tris, pH 7.2	10 mM
Urea	8 M
NaCl	1 M

The eluate was again collected in fractions and those were analysed with a Coomassie gel. The fractions containing the highest amount of purified NM were pooled and dialysed twice against 5 L of PBS. The protein concentration was determined according to the Lambert-Beer law and aliquots were stored at -80°C. Immunochemical confirmation of the purification of NM was performed via Western blot.

Recombinant Sup35NM used in our experiments was previously produced by dr. Julia Hofmann in the laboratory of AG Vorberg, DZNE. Expression and purification protocols are described in [43].

We expressed the recombinant Sup35NM-His using pJ404-NM (purchased from DNA 2.0) as previously described. Protein was purified using Ni-NTA resin with Äkta purifier.

4.3.2. Fibrillization of recombinant NM protein

To prepare NM fibrils, soluble recombinant NM protein (100 µM) was thawed at room temperature and transferred into a new protein LoBind tube. The protein was either first diluted to 10 µM in PBS or undiluted rotated for 24 hours at 4°C or room temperature, at 50 rpm to induce fibrillization of NM. Fibrils were sonicated for 3 minutes at 10% power (1 second on/0.5 second off) prior to use [44].

4.4 Cell biological methods

4.4.1. Cryoconservation and thawing of cells

Cryoconservation of cells in liquid nitrogen was used for long term storage of immortal cells. On Mondays a vial containing 1 ml 6.5×10^6 NM-GFP cells was thawed at 37°C in water bath for 1 minute and added to 9 ml prewarmed cell medium. Cells were pelleted at 150 xg for 3 minutes at 4°C. The supernatant was aspirated and 10 ml fresh medium was added. The cell suspension was seeded in the T175 culture flask, containing 25 ml prewarmed medium.

4.4.2. Cultivation and passaging of N2a cells

The mouse neuroblastoma cell line N2a was maintained in Opti-MEM medium containing 10% FCS, penicillin and streptomycin (60U/ml). Cells were split on Mondays, Wednesdays and Fridays and were passaged no more than sixteenth passages. For passaging, medium was aspirated and cells were rinsed with 15 ml PBS and treated with prewarmed trypsin/EDTA (3 ml) for 3 minutes. Afterwards, flasks were gently tapped to detach cells. Cell suspensions were prepared by adding prewarmed medium (17 ml) and by pipetting up and down ten times. For further culture, 5×10^6 cells were seeded on Mondays and Wednesdays, and 1.8×10^6 cells on Fridays in T175 flask to a total volume of 35 ml. Cells were grown at 37°C in a 5 % CO₂ atmosphere for 48 or 72 hours, respectively.

4.4.3. Determination of cell number

The cell number was determined either with Vi-CELL (Beckman Coulter) or by using a TC20™ automated Cell Counter (Bio-Rad) with dual chamber counting slides. Both work on the same principle. The cell suspension was mixed 1:1 with trypan blue to stain for dead cells. The cell counter recognizes cells according to their shape and size and dead cells based on trypan blue stain. The live cell number per ml was determined and used for further experiments.

4.5 Quantification of intracellular aggregates prior to fibril exposure

4.5.1. Reverse method

A tube of 100 μM NM protein was rotated at 4°C for 24 hours to produce fibrils. Fibrils were subsequently sonicated according to the fibrillization protocol. Produced fibrils were diluted to a concentration of 1 μM (monomer concentration) and added to the 6-well plate for seeding. After 8 hours, 4×10^5 cells were added on top of the fibrils. After 24 hours, cells were harvested and 7×10^4 seeded onto the 96-well plate for nuclei staining and microscopy.

4.5.2. Aggregate induction assay

The N2a cells expressing soluble NM-GFP were seeded onto the 6-well plates (4×10^5 /48 hours), 96-well plates (1×10^4 /24 hours) or 384-well plates (1×10^4 /12 hours) and incubated at 37°C, in a 5 % CO₂ atmosphere for 2-24 hours. NM fibrils were added to the cells at a final concentration of 1 or 10 μM (monomer equivalent) and cells were further incubated for 12-24 hours. After incubation they were fixed either in 4% paraformaldehyde for 20 minutes at 37°C and immediately stained with Hoechst or fixed using 1% paraformaldehyde and incubated at 4°C overnight.

4.5.3. Determination of optimal cell seeding number and time for aggregate induction assay

For determination of optimal cell seeding density for the aggregate induction assay, different cell numbers were seeded onto the 96 or 384-well plates. Plates were scanned with Cell Voyager (CV6000) and the optimal cell seeding density was defined based on the 90% cell layer confluency. To determine the optimal seeding time before addition of the NM fibrils, the induction rate of 6 different seeding times (0, 2, 4, 6, 8 and 10 hours) were measured. For this purpose, cells were splitted and seeded every 2 hours, and further incubated for 14, 17, 20 or 22 hours. Subsequently, cells were fixed in 1% paraformaldehyde and incubated at 4°C overnight.

4.5.4. Nuclei staining and automated confocal microscopy

The nuclei stainings of cells on 96 and 384-well plates were performed using the Biomek® FXP Laboratory Automation Workstation. Fixed cells were permeabilized with 0.5% Triton X-100 for 30 minutes. Subsequently, the nuclei were stained with 4 μg/ml Hoechst dye for 15 minutes and washed twice for 5 minutes with PBS. Cells were scanned with Cell Voyager (CV6000) at 10x, 20x or 40x magnifications, with 488 nm and 405 nm lasers.

4.5.5. Image and statistical analysis

Images from CV6000 were analysed either with the Columbus™ Image Data Storage and Analysis System program or the Cell Voyager Analysis Support Software from Yokogawa. A script was developed to find nuclei, cell region and the aggregates. Additional parameters such as cell circularity, cell area, total cell number, green cell number and cells with aggregates were also included. Circularity defines the roundness of the nuclei, increase of which together with decreased cell size and reduced cell number serves as an indication for the cytotoxicity.

4.5.6. Statistical analysis

Statistical analyses for the aggregate induction assay were performed using the Graph Pad Prism software. Each experiment was performed at least in duplicates. Statistical significance was analysed with Chi-square test with an alpha error value of 5%. P-values higher than 0.05 were not considered to be significant. Significant values were marked with *($p \leq 0.05$), **($p \leq 0.01$), ***($p \leq 0.001$) and ****($p \leq 0.0001$). Error bars represent the standard error of mean (SEM).

4.6 Screen

The screen for aggregate induction assay was performed to test if the established protocols were amenable to automated plate processing. An automated processing routine was developed in collaboration with the DZNE high content screening facility. As shown in Figure 6, cells were allowed to settle for 1 hour and then treated with compounds for 1 hour, before addition of NM fibrils. Cells were further incubated for 12 hours, fixed in paraformaldehyde, then scanned with CV6000 and analysed with the Yokogawa software. Statistical analysis for the screen were performed by the DZNE high content screening facility.

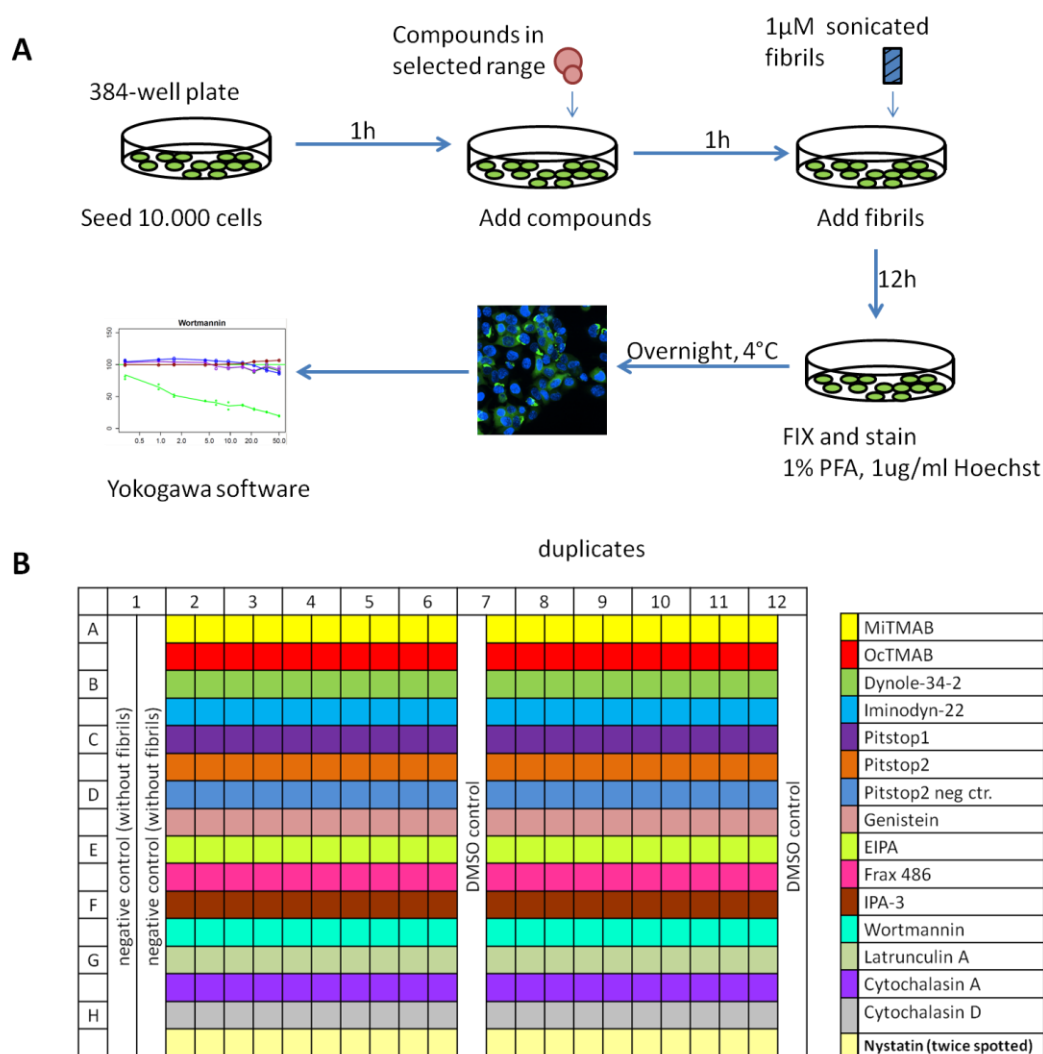


Figure 6: Work flow for screening. (A) 10.000 cells were seeded into the 384-well plate. After 1 hour incubation for cell attachment, compounds in 10 different concentrations in duplicates were added to the plate and incubated for additional 1 hour. Prepared fibrils were added for further co-incubation of 12 hours. Cells were fixed and stained in 1% paraformaldehyde (PFA) and 1μg/ml Hoechst at 4°C overnight. (B) Layout of the screening plate.

4.6.1. Compound preparation (activators and inhibitors of different endocytic pathways)

Compounds were dissolved in water or in the DMSO to the stock solution and stored either at +4°C or -20°C according to the distributor's recommendations.

Table I: Endocytosis activators and inhibitors

	Compound	stock	solvent	Distributor
1	U18666A	10mM	H ₂ O	Sigma
2	Ammonium chloride (NH ₄ Cl)	5M	H ₂ O	Sigma
3	Chloroquine diphosphate salt (CQ)	10mM	H ₂ O	Sigma
4	Epidermal growth factor (EFG)	10µg/ml	DMSO	Sigma
5	MiTMAb	10mM	DMSO	Abcam
6	OctMAb	10mM	DMSO	Abcam
7	Dynole-34-2	10mM	DMSO	Abcam
8	Iminodyn-22	10mM	DMSO	Abcam
9	Pitstop1	25mM	DMSO	Abcam
10	Pitstop2	25mM	DMSO	Abcam
11	Pitstop2 neg ctr.	25mM	DMSO	Abcam
12	Nystatin	5mM	DMSO	Sigma
13	Genistein	50mM	DMSO	Enzo
14	EIPA	25mM	DMSO	Enzo
15	IPA-3	25mM	DMSO	Sigma
16	FRAX486	10mM	DMSO	Tocris
17	Wortmannin	10mM	DMSO	Tocris
18	Latrunculin A	1mM	DMSO	Tocris
19	Cytochalasin D	1mM	DMSO	Tocris
20	Cytochalasin A	1mM	DMSO	Enzo

4.6.2. Compound spotting using the Echo 550 system

Compound stock solutions were added to the source plate, from where the Echo 550 Liquid Handler (Labcyte) automatically spotted different volumes to the destination plate. Volumes from 2.5 nl up to 400 nl were used to reach the expected compound concentrations diluted in medium. From the destination plate, 10 µl of the compounds were transferred to the screening plate, seeded with cells, for compound treatment.

MATERIAL

4.7 Chemicals

Coomassie brilliant Blue	Roth, Germany
Dimethyl sulfoxide (DMSO)	Sigma-Aldrich, Germany
Ethanol 99 %	Roth, Germany
Ethylen diamine tetraacetate, sodium salt	Roth, Germany
Glycerol	Roth, Germany
Glycine	Roth, Germany
HCl 37 %	Roth, Germany
Hoechst 33342, trihydrochlorid, trihydrate	Sigma-Aldrich, Germany
LB Broth agar	Sigma-Aldrich, Germany
Methanol	Roth, Germany
Paraformaldehyde	Roth, Germany
Phosphate buffered saline (PBS)	Invitrogen, Germany
Q Sepharose fast flow	GE Healthcare, Germany
Skimmed milk powder	Roth, Germany
Sodium bicarbonat	Sigma-Aldrich, Germany
Sodium chloride (NaCl)	Roth, Germany
Sodium hydroxide	Roth, Germany
Tris-hydroxy-methyl-aminomethan (Tris)	Roth, Germany
Triton X-100	Sigma-Aldrich, Germany
Urea	Roth, Germany

4.8 Consumables

Cryotubes	Corning, USA
Filter system, 500 ml (431097)	Corning, USA
Mini Protean Tetra System	Bio-Rad, Germany
Multiwell Plates BD	Biosciences, Germany
Nitrocellulose Membrane	GE Healthcare, Germany
Pipets (0.5-10 µl, 10-100 µl, 100-1000 µl)	Eppendorf, Germany
Protein LoBind Tube	Eppendorf, Germany

Rotilaber Blotting Paper	Carl Roth, Germany
SafeSeal-Tips (20 µl, 100 µl, 1000 µl)	Biozym, Austria
Stripette (5 ml, 10 ml, 25 ml)	Corning, USA
Tube (1,5 ml; 2 ml)	Eppendorf, Germany
Tubes (15 ml, 50 ml)	Falcon, France
µclear-plate, Black, 96 well	Greiner, Germany

4.9 Cell Culture Medium and Supplements

Fetal calf serum (FCS)	Invitrogen, Germany
Opti-MEM	Invitrogen, Germany
Penicillin/Streptomycin	Invitrogen, Germany

4.10 Instruments and Accessories

ÄktaFPLC	GE Healthcare, Germany
Automated cell counter TC20	Bio-Rad, Germany
Biomek®FXP Laboratory Workstation	Beckman Coulter, Germany
CO ₂ Incubator	Haraeus, Germany
Echo® Liquid Handler for Screening	Labcyte, USA
Electrophoresis Power Supply Consort	Turnhout, Germany
Eppendorf 5417C	Eppendorf, Germany
Fluostar Omega BMG	Labtech, Germany
Lab-Therm CT-X Kühner schaker,	Birsfelden, Switzerland
Multidrop™ Combi Reagent Dispenser	Thermo Scientific, Germany
Multifuge X3R Hereus	Thermo Scientific, Germany
Nanodrop 2000c	Thermo Scientific, Germany
pH-Meter Seven Easy	Mettler-Toledo, Germany
Scanlaf Mars Safety Class 2	Labogene, Denmark
Sonicator Sonoplus HD 3200	Bandelin, Germany
Stella	Raytest, Germany
Thermomixer compact	Eppendorf, Germany
Vi-Cell	Beckman Coulter, Germany

4.11 Microscopes

Cell Voyager 6000	Visitron Systems GmbH, Germany
Leica DM IL LED Fluor 297 microscope	Leica, Germany
Leica DM IL LED microscope	Leica, Germany

4.12 Software

Adobe Illustrator CS6	Adobe Systems, USA
Cell Voyager Analysis Support Software	Visitron Systems GmbH, Germany
ExpASY Bioinformatics Resource Portal SIB	Swiss Institute of Bioinformatics
GraphPad Prism 6	Graph Pad Software, USA
Microsoft Excel 2010	Microsoft, USA
Microsoft Word 2010	Microsoft, USA
Zen 2011 (blue edition)	Carl Zeiss, Germany

4.13 Other used material

Escherichia coli BL21/DH5 α

N2a (mouse neuroblastoma cells); 89121404 ECACC	Sigma-Aldrich, Germany
Ampicillin (Amp)	Sigma-Aldrich, Germany
Page Ruler prestained Protein Ladder	Thermo Scientific, Germany

Buffers and solutions are included in method description

5 RESULTS

5.1 Establishment of a cell-based aggregate induction assay for a high content screen

We have previously established a cell-based aggregate induction assay based on the ectopic expression of the yeast Sup35 prion domain in the cytosol of mammalian cells [43, 44]. In this cell-based aggregate induction assay, pre-formed recombinant NM fibrils were applied to the mammalian N2a cells expressing soluble cytosolic homotypic protein tagged with the green fluorescent protein (NM-GFP^{sol} cells). After an incubation time, green aggregates were observed in NM-GFP cells (NM-GFP^{agg} cells). In order to identify possible mechanisms involved in the aggregate induction, the aim of this study was to adapt the assay to 384-well format and to optimise it to obtain robust and highly reproducible results for high content screening. For this purpose, the experiments were first performed in 6-well and 96-wells and further carried on with the 384-well plate, which is suitable for the screen. Various parameters were optimised to define the ideal conditions: cells seeding, compound pre-incubation time, fibril co-incubation time, scanning and image analysis protocols.

For a robust assay, a standardized fibril production protocol and high induction rates are essential. Thus, NM fibril rotation protocols as well sonication protocols were established. Subsequently, fibril rotation concentration and working concentration were defined. For ideal cell culture conditions, parameters such as cell passage number and seeding concentration of the cells were optimised. Additionally, some possible compounds and various protocols to increase the cellular uptake were tested for their possible effects on the aggregate induction rate. Finally, optimal compound concentrations and solvent concentrations were defined.

5.1.1. Sonication of the NM fibrils increases the aggregate induction rate in the NM-GFP cells

In yeast, the heat shock protein Hsp104 is crucial for the maintenance of Sup35 prion state, since it cleaves larger aggregates into smaller seeds, which are required for the Sup35 nucleation [56]. Either excess or insufficient Hsp104 perturb the aggregation process and eliminate the Sup35 prion state [56]. Sonication has been shown previously to break fibrils formed *in vitro* into smaller fragments that might have a higher induction activity [43]. To

prove that sonicated NM fibrils can increase induction efficiency in our cell-based aggregate induction assay, different concentrations of recombinant NM monomer in PBS were rotated at 4°C for 24 hours. Produced fibrils were either sonicated or left on ice before adding them to the cells. Figure 7 shows the percent of NM-GFP^{agg} cells with green aggregates induced by the fibrils rotated at different rotation concentrations (monomer equivalent): 10 μM (green bars), 20 μM (blue bars) and 50 μM (orange bars). The working concentration of fibrils added to the cells in this experiment was 1 μM (monomer equivalent).

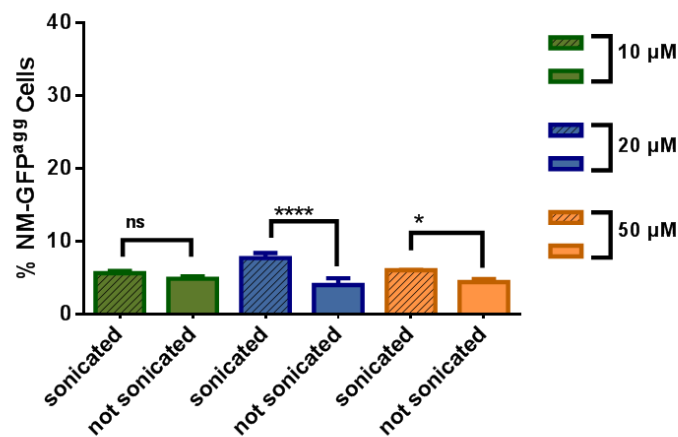


Figure 7: Sonication of fibrils increases the endogenous aggregate induction rate. Graph represents the percent of NM-GFP cells with green aggregates (NM-GFP^{agg} cells). Samples are divided into three groups according to the different rotation concentrations. Green, blue and orange bars demonstrate the results obtained with 10μM, 20μM and 50μM concentration of the rotated NM protein diluted in PBS, respectively. First of the two bars from each group indicates a sonicated (10% power; 1 second on/0.5 second off; 3 minutes) and second a non-sonicated samples performed in duplicates. Error bars represent the SEM. Chi-square test: ****p≤0.0001; *p≤0.05; ns, not significant.

Usually, at least 5% of NM-GFP cells contained green aggregates. Experiment with sonicated and non-sonicated samples demonstrated that with all three different rotation concentrations, sonicated fibrils induced aggregation in a higher percentage of cells than non-sonicated fibrils. In the second and the third group the differences between these two samples were significant. From these data we conclude that sonication is an important step in this assay and can increase the aggregate induction efficiency. Thus, overnight rotated and sonicated fibrils were used in all further experiments. On the other hand, no difference was observed between the three groups with distinct rotation concentrations.

5.1.2. Chloroquine diphosphate salt is a prominent aggregate induction activator

For high content screening a robust assay with high aggregate induction rate is crucial. Since the percent of the NM-GFP^{agg} cells was very low (around 5%), our interest was to increase the aggregate induction in these cells by increasing the fibril uptake or preventing potential degradation of aggregates in the endo-lysosomal system. For this purpose, we tested four chemical compounds, known to either increase the cellular uptake or impair lysosomal proteolysis. NM-GFP cells were treated with U18666A (amphipathic steroid), chloroquine diphosphate salt (CQ), ammonium chloride or epidermal growth factor (EGF) in various concentrations to test their effects on the fibril aggregate induction. The U18666A inhibits intracellular cholesterol trafficking from endosomes and lysosomes [57]. CQ and ammonium chloride also interfere with endosome- lysosome system. They inhibit the acidification of the aforementioned system and have been suggested to slow down the proteolytic degradation of the endocytosed particles [57]. EGF is a growth factor that stimulates proliferation, differentiation and cell growth by binding to the epidermal growth

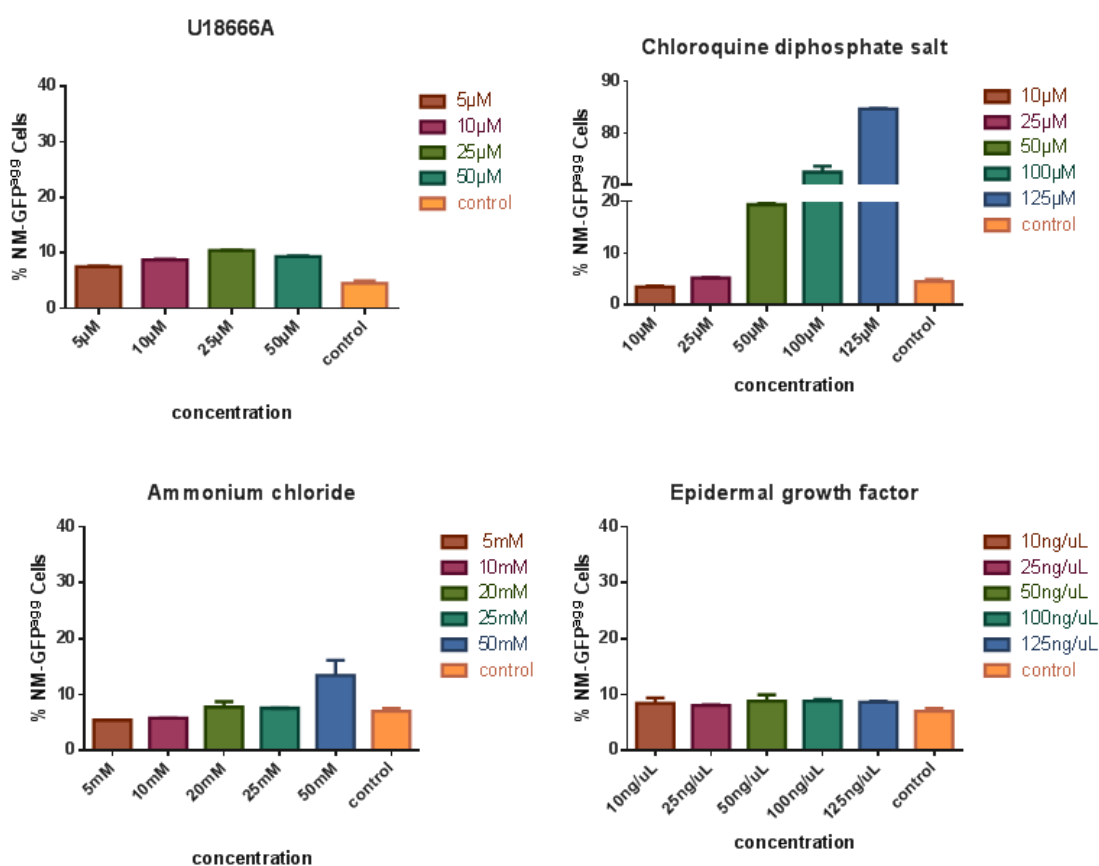


Figure 8: Impact of the compounds on the NM-GFP protein aggregate induction. These graphs represent the percent of NM-GFP cells with green aggregates treated with chemical compounds and 1 μM (monomer equivalent) fibrils. All treatments were performed in duplicates. Error bars represent the SEM.

factor receptor. It was proposed to induce macropinocytosis, the major endocytic pathway for internalising large cargo [58]. According to the literature, four different concentrations for U18666A were chosen between 5 μ M and 50 μ M [59]. For CQ, five concentrations in the range from 10 μ M to 125 μ M [60], for ammonium chloride five concentrations from 5 mM to 50 mM [60] and for EGF five concentrations starting at 10 ng/ μ l and up to 125 ng/ μ l were tested. NM-GFP cells of the 9th passage number were treated with different compounds and aggregates were induced with 1 μ M (monomer equivalent) prepared fibrils.

The control cells were treated with 1 μ M (monomer equivalent) fibrils in DMSO (solvent control). Compared to this control (\approx 5% NM-GFP^{agg} cells), a two-fold increase in aggregate induction was observed with 25 μ M and 50 μ M U18666A. Similar to U18666A, also 50 mM ammonium chloride led to increased aggregate induction (\approx 10% NM-GFP^{agg} cells). The strongest increase was observed in the CQ treated cells. CQ drastically enhanced aggregate induction already at low concentrations and led to up to 85% of cells with green aggregates (Figure 8). Additionally, a large number of vacuoles were observed in the CQ treated cells (Figure 9), potentially representing lysosomes. While, the previously mentioned three compounds all increased the aggregate induction, EGF did barely affect the induction rate in our experiments.

In conclusion, chloroquine diphosphate salt is an effective activator in the NM aggregate induction assay, especially when used at higher concentrations (50-125 μ M). However, due to its strong effect on cell morphology it was decided not to use it in the following optimisation protocol.

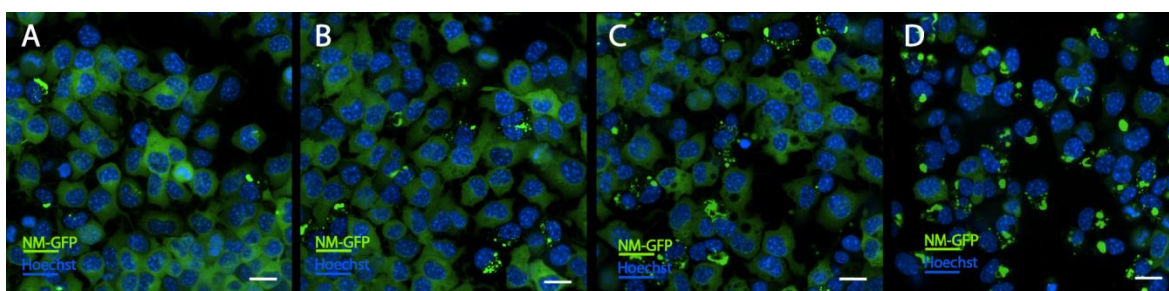


Figure 9: Chloroquine diphosphate salt (CQ) drastically increased the percentage of cells with green aggregates (NM-GFP^{agg} cells). (A) In the control well, NM fibrils induced aggregation in about 5% cells. (B) Cells treated with 25 μ M CQ contained 8% NM-GFP^{agg} cells. (C) Cells treated with 50 μ M CQ had 20% NM-GFP^{agg} cells with large vacuoles. (D) Cells treated with 100 μ M CQ contained 75% NM-GFP^{agg} cells. At concentration \geq 100 μ M, almost all cells were induced. Nuclei were stained with Hoechst (blue) and cells expressed NM tagged with GFP (green). Bar scale represent 20 μ m.

5.1.3. NM seeds produced by rotation at 4°C exhibit a higher aggregate induction activity than fibrils produced at room temperature

Our previous data showed that *in vitro* mature fibril formation is completed within 24-48h [25]. Classically, all of the experiments were performed with fibrils rotated at 4°C. Previous *in vitro* experiments by other groups have demonstrated that NM readily forms fibrils also when rotated at room temperature [61]. To test whether NM fibrils have better induction efficiency when rotated at 4°C than at room temperature, NM protein was rotated in parallel under both conditions. This experiment was performed with NM-GFP cells of 10th passage number and 16th passage number. NM fibrils with 10 µM or 100 µM (monomer equivalent) rotating concentrations and a final working concentration of 1µM (monomer equivalent) were applied to the cells. Initially the aggregate induction assay yielded around 5% of NM-GFP cells with aggregates.

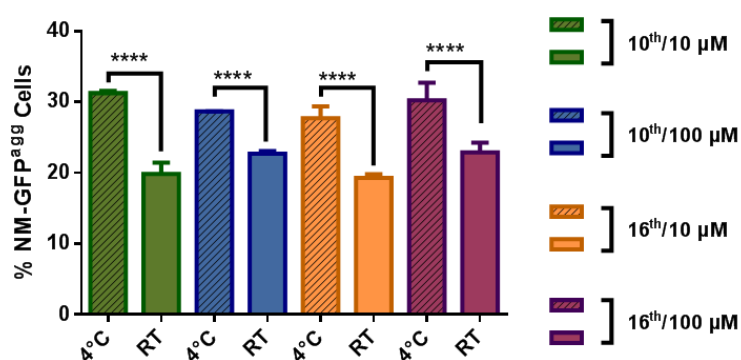
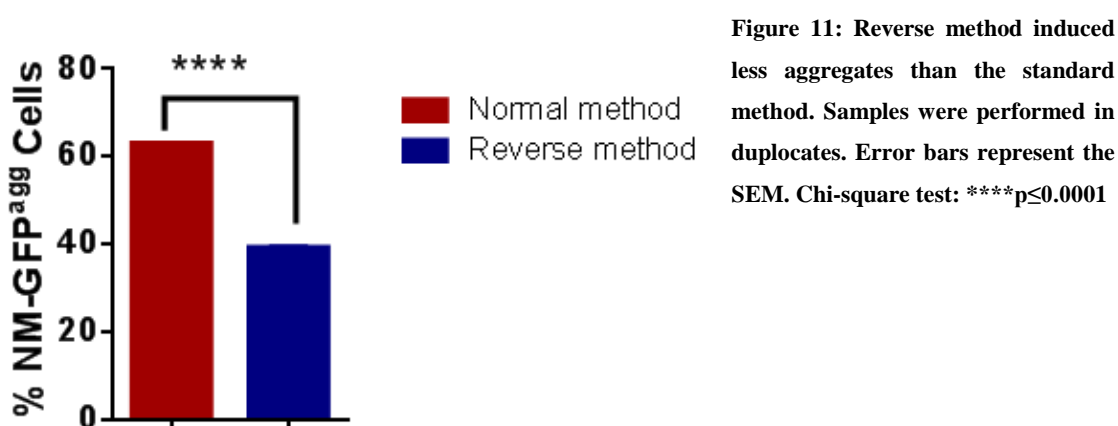


Figure 10: Fibrils rotated at 4°C display a higher aggregate induction activity. Samples were divided into four groups according to the NM monomer rotation concentration (10 µM or 100 µM) and cell passage number (10th or 16th). Graph represents percent of NM-GFP^{agg} cells with green aggregates in green (10th/10 µM), blue (10th/100 µM), orange (16th/10 µM) and violet (16th/100 µM). All wells were treated with 1 µM prepared fibrils and experiments were performed in duplicates. Hatched bars from each group represent samples treated with fibrils rotated at 4°C; solid bars represent samples treated with fibrils rotated at room temperature (RT). Error bars represent the SEM. Chi-square test: ****p≤0.0001

Due to following standard operating procedures, aggregate induction rate in this experiment was increased up to 30%. All groups showed a significant decrease in cells with green aggregates when cells were treated with fibrils rotated at the room temperature. For different rotation concentrations, similar to previous results, no difference was observed. For convenience, 100 µM (monomer equivalent) undiluted NM protein was used for further experiments. In conclusion, fibrils rotated at 4°C have better aggregate induction efficiency and induce more NM-GFP cells to form green aggregates.

5.1.4. Reverse method with pre-adsorbed fibrils decreases induction efficiency

In some virus uptake studies, a reverse method, in which viral particles are adsorbed to the test plate, has been proven to be more efficient than classical virus application on the top of the cells [62]. Due to a high local concentration of viral particles using the reverse method, the particles applied by this method might have better prospect to enter the cells. To investigate the effect of the reverse method in our aggregate induction assay, rotated fibrils were adsorbed to the assay plate for eight hours, and cells were subsequently added on top of the fibrils and further cultivated overnight.



In this experiment more than 60% NM-GFP cells included green aggregates even in the controls, likely due to the standard operation procedures. Surprisingly, the reverse method resulted in a lower aggregate induction rate. According to this fact, our further experiments were performed using the standard method.

5.1.5. Higher N2a NM-GFP cell passage number has no significant effect on the aggregate induction

To test whether a higher passage number affects the fibril aggregate induction rate, cells from different passages post thawing were tested. Figure 12 shows two individual experiments including cells of different passage numbers treated with 1 μM (green bars) or 10 μM (blue bars) fibrils (monomer equivalent). A trend was observed that higher passage number led to increased aggregate induction, suggesting that cells that had been in culture for longer were slightly more efficient in aggregate induction. Higher n numbers are required to test this hypothesis. To ensure robust cell treatment to avoid intra-assay

variability, we used the 4th passage of NM-GFP cells for our further experiments. During the assay optimisation, the aggregate induction rate increased from initial 5% to 10%, in later experiments up to 50% due to proper fibril production protocol and standard cell culture methods. Thus, the data were only compared within the same experiment.

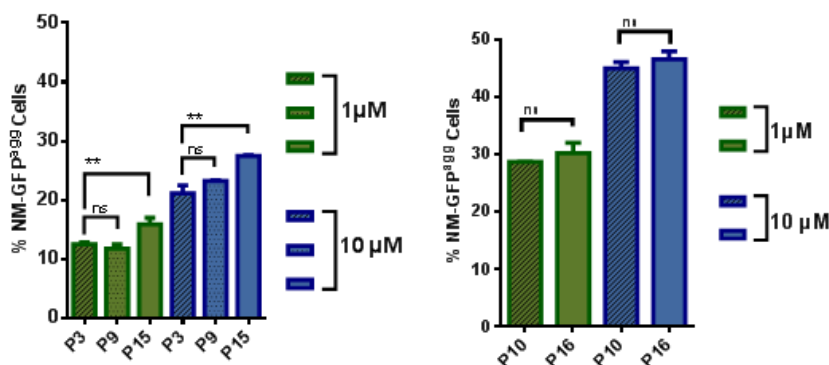


Figure 12: Higher passage does not influence the aggregation rate in NM-GFP cells. Graphs present two individual experiments. Bars represent the percent of NM-GFP^{agg} cells with green aggregates. Samples were divided into two groups according to the working concentration of fibrils. While the first group (green) was treated with 1 μM prepared fibrils, the second group (blue) was treated with 10μM fibrils (monomer equivalent). Different bars present various passage (P) numbers. All experiments were performed in duplicates. Error bars represent the SEM. Chi-square test: **p<0.01; ns, not significant.

5.1.6. Optimised cell pre-seeding and fibril incubation time in the aggregate induction assay

In the foregoing experiments, cells were pre-seeded one day before fibril application, and were further incubated with fibrils for another 24 hours. To optimise the protocol, the optimal cell seeding time and fibril incubation time were determined. For this purpose, cells were seeded onto the plate for 0 to 10 hours in two hour intervals and further incubated with fibrils for four different periods: 14, 17, 20 and 22 hours. The classical 24 hours cell pre-seeding and 24 hours 1 μM (monomer equivalent) NM fibril induction protocol was utilized as a control protocol. Our results revealed no significant difference in aggregate induction rate between different protocols (Figure 13A). As negative control, 24 hours pre-seeded cells without additional fibril application was used. For convenience, the protocol with 2 hours pre-seeding and 12 hours fibril incubation was chosen for the screen.

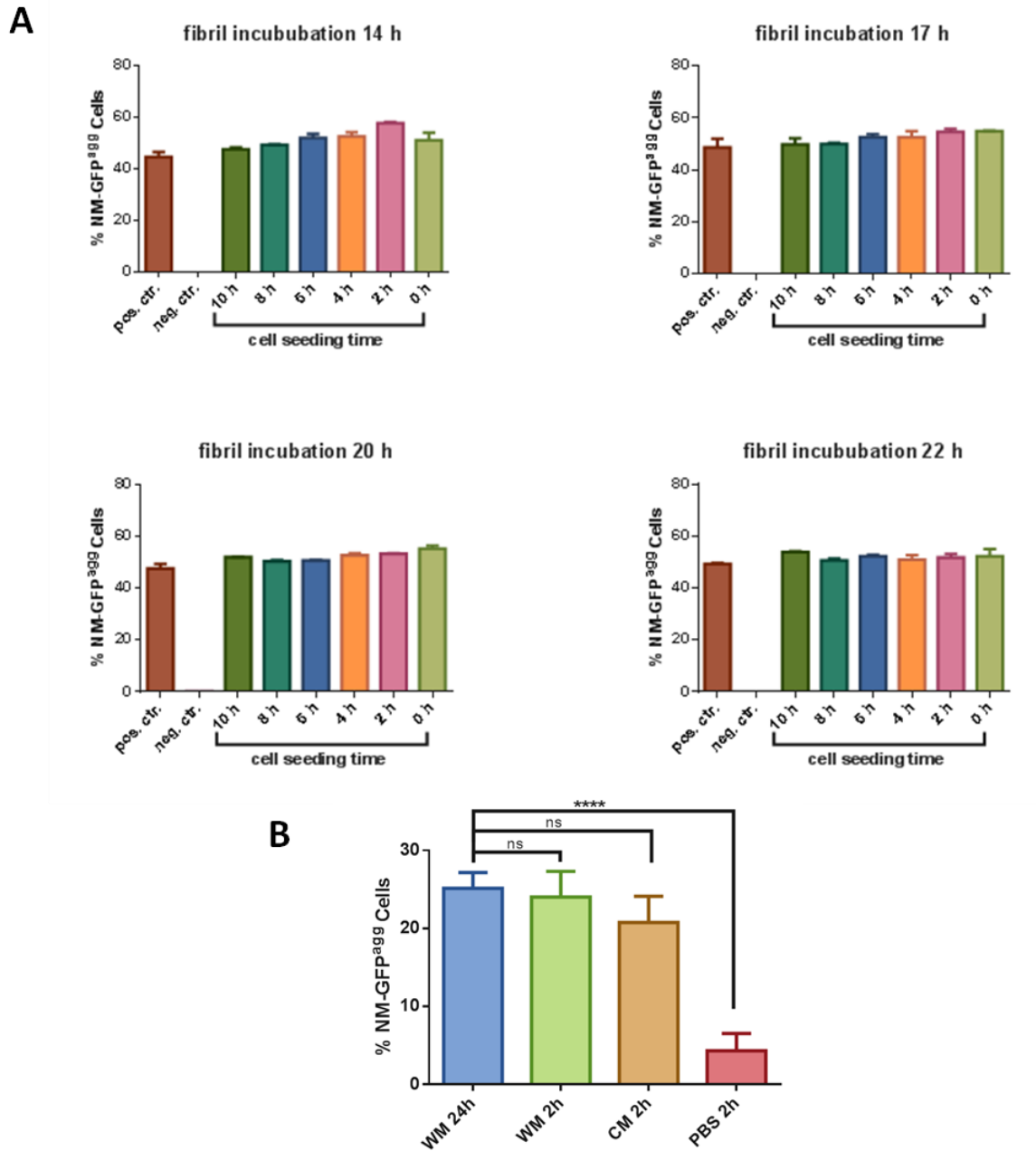


Figure 13: Optimal cell seeding time prior to fibril application and fibril incubation time in the aggregate induction assay. (A) The four graphs represent four different fibril incubation times (14, 17, 20 and 22 hours). Each bar in the graph corresponds to the cells seeded 0, 2, 4, 6, 8 or 10 hours before fibril application. Positive control represents NM-GFP^{agg} cells seeded for 24 hours before fibril exposure (brown bar) and negative control represents NM-GFP^{agg} cells without fibril addition. **(B)** Fibrils were diluted in warm medium (WM), cold medium (CM) or PBS. Control (WM24h) represent the fibrils diluted in warm medium and applied on the cells, which were seeded 24 hours before. The second, third and fourth bar represent cells seeded 2 hours before fibril exposure (0.25 μ M monomer equivalent). All the samples were performed in duplicates. Error bars represent the SEM. Chi-square test: ****p<0.0001; ns, not significant.

Normally we use warm medium as dilution agent for the fibrils. Here, additionally, warm growth medium, cold growth medium and PBS were tested to define the best dilution agent. In Figure 13B, the growth medium (cold and warm) diluted fibrils induced significantly more aggregates than the PBS diluted fibrils. Thus, fibrils should be diluted into the growth medium before application.

5.2 Screen with endocytic inhibitors reveals that macropinocytosis is involved in NM aggregate induction

An optimised aggregate induction assay was now used to identify endocytic pathways involved in the aggregate induction. For this purpose, 100 μM (monomer equivalent) of recombinant NM protein was thawed and rotated at 4°C for 24 hours to form mature fibrils. Prior to fibril application 10.000 cells per well were pre-seeded onto the 384-well for one hour, then treated with compounds for one hour before fibrils application. After sonication, fibrils were diluted into the warm growth medium and applied to the cells at a concentration of 1 μM (monomer equivalent). Cells of 4th passage were used for the screen. No additional activators were used to avoid any possible compound effects. Cells were treated with fibrils and compounds for additional 12 hours. The optimised aggregate induction assay yields 50% NM-GFP^{agg} cells, which is reproducible.

To test the feasibility of this assay, a small screen with endocytic inhibitors was performed. Endocytosis is the major process for the cellular uptake. It contains three major pathways: Clathrin-dependent, caveolae-dependent pathways and macropinocytosis. To investigate which endocytic pathways are involved in the aggregate induction, 15 specific endocytic inhibitors were tested. These include four dynamin inhibitors, two compounds inhibiting clathrin pit formation, five macropinocytosis inhibitors, three cytoskeleton disruptors and one caveolae/lipid rafts inhibitor. Different concentrations of the compounds were used for dose-response curves. The concentration ranges of the compounds were chosen based on the literature search of effective compound concentrations in cell-based assays or based on recommendations of the manufacturer. The highest concentration used was 160-times higher than the lowest. A positive control with fibrils and DMSO solvent, and a negative control with only DMSO treatment without fibrils, were included. The experiment was performed twice in duplicates and the average aggregate induction rate was normalized

against the positive control to negate the DMSO effect and variations between experiments. The aggregate induction assay was performed on 384-well plates and was fully automated.

Important criteria for cytotoxicity were the reduction of the number of NM-GFP cells by 10% and increased cell circularity by 10% compared to the positive control. Cell area was also included in the image analyses program, which usually followed the decreased percentage of NM-GFP cells and indicated the compound effect on the cell viability. As shown in Figure 14, cells treated with 0.1% DMSO alone showed no aggregation of the NM-GFP protein and cytotoxicity. Unlike, in fibril treated samples aggregation of the homotypic protein was induced in 50% of NM-GFP cells. The results were validated in two independent screens with identical results.

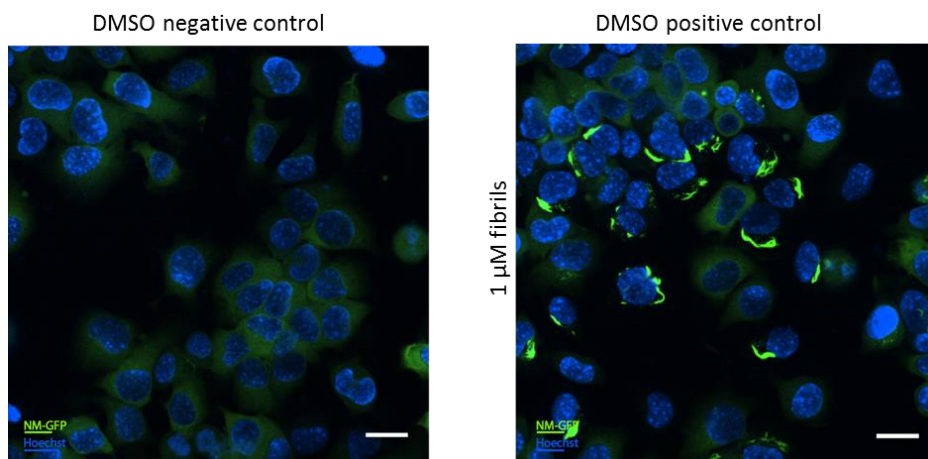


Figure 14: DMSO controls. Positive DMSO control (right) with added fibrils induced the NM aggregation, whereas in cells without fibril treatment (left) cytosolic NM-GFP protein remained soluble. Bar scales represent 20 μm .

5.2.1. Latrunculin A, cytochalasin A and cytochalasin D reduce the aggregate induction rate

Latrunculins and cytochalasins are commonly used actin-depolymerization agents in endocytic studies [63]. They destabilize the actin filaments and accelerate the actin disassembly by binding to the actin monomers or the fast growing end of actin filaments, respectively [63, 64]. These very potent, membrane-permeable actin-disrupting agents were used in concentrations ranging from 0.03 μM to 5 μM . As shown in Figure 15 and 16, aggregate induction rates (GreenAggRatio) in cells treated with latrunculin and

cytochalasins were drastically decreased already at low concentrations and continuously dropped with increased concentrations. This demonstrated that treatment with actin-depolymerization agents decreases the percentage of cells with green aggregates. Furthermore, at middle range concentrations ($\approx 0.15 \mu\text{M}$), cells showed a tendency to cluster and to form several hundred micrometres long “chains”. Cytochalasin A ($>0.4 \mu\text{M}$) induced dramatic changes in the morphology of the cells. Cells became round, condensed

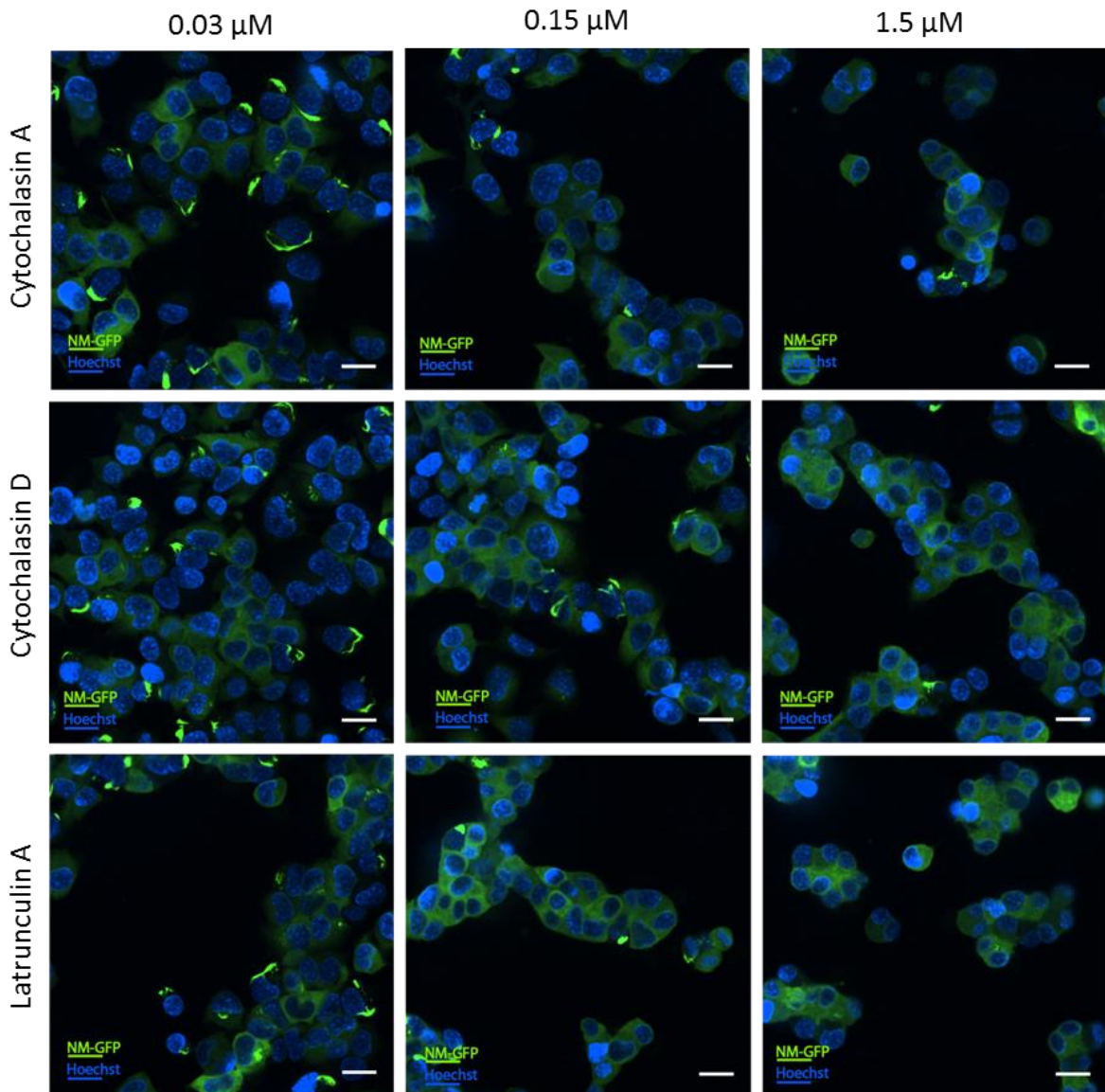


Figure 15: Latrunculin A, cytochalasin A and cytochalasin D treated cells. In the first column cells treated with $0.03 \mu\text{M}$ are shown, whereas the second and third images show cells treated with $0.15 \mu\text{M}$ and $1.5 \mu\text{M}$ compounds, respectively. Compound concentration $> 0.15 \mu\text{M}$ influenced cell formation. Cells had the tendency to clump and formed long chains, containing 5-30 cells, which increased with compound concentration. Bar scale represent $20 \mu\text{m}$.

and were most probably dead. Shown in Figure 16 cell area and cell number for cytochalasin A decreased with the % of NM-GFP^{agg} cells along the dose-response curve. The same effect was observed in cells treated with cytochalasin D at concentrations higher than 1 μ M. Similar to cytochalasins, also latrunculin A decreased the cell viability, already when cells were treated with concentrations higher than 0.1 μ M.

In summary, these results suggest that the NM-GFP protein aggregate induction in N2a cells is actin-dependent. The cytoskeleton is involved in almost all of the endocytic routes including macropinocytosis, clathrin and caveolae-dependent pathways as well as in other clathrin independent uptake mechanisms, suggesting that actin inhibition could also impair NM fibril uptake. Additionally, these compounds disrupt the actin polymerization in the μ M concentration range, thus affecting the cell morphology and cell viability.

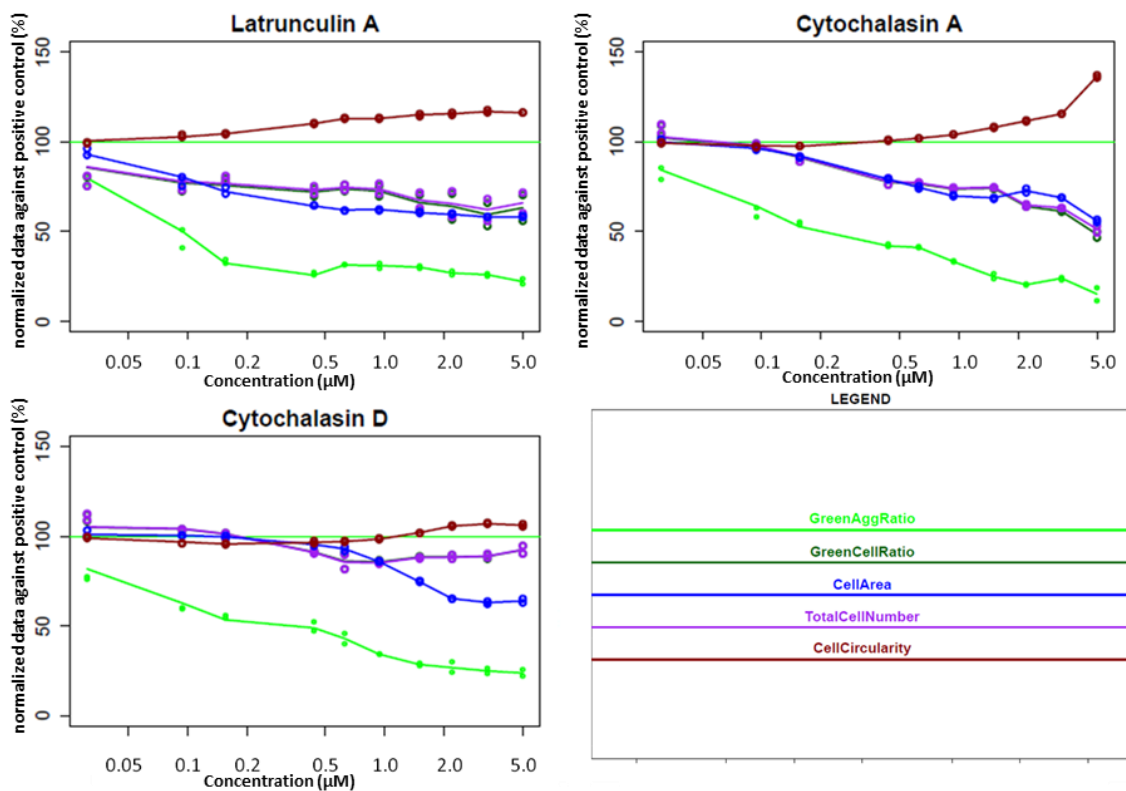


Figure 16: Dose response curves for latrunculin A, cytochalasin A and cytochalasin D. Curves clearly showed decreased aggregate induction and increased cytotoxicity with concentration. Red: cell circularity, violet: total cell number, dark green: green cell number, blue: cell area, light green: number of green aggregates.

5.2.2. Dynamin inhibitors slightly increase the aggregate induction rate

Receptor mediated endocytosis usually occurs via clathrin and/or caveolae-dependent pathways [65], for which ubiquitously expressed dynamins are required. Dynamins are large GTPases responsible for pinching off the newly formed vesicles from the cell membrane [48]. Compounds like MitMAB, OctMAB, dynole and iminodyn are potent, cell permeable dynamin inhibitors used to study the clathrin- and caveolae-dependent endocytosis [65]. In our experiment, cells were incubated with dynamin inhibitors at concentrations between 0.3 μM and 50 μM to block the clathrin and caveolae-dependent pathways (Figure 17 and 18). Data analysis revealed approximately 15% increase of NM-GFP^{agg} cells at concentration up to 5 μM for OctMAB and dynole. The same effect was observed in cells treated with iminodyn at concentrations lower than 2 μM and in cells treated with MitMAB at concentrations lower than 10 μM . By OctMAB, iminodyn and MitMAB the aggregate induction rate was drastically decreased above a certain concentration, or in case of dynole, it was first increased and then decreased. Since compounds at these concentrations were extremely cytotoxic, results were considered as not specific.

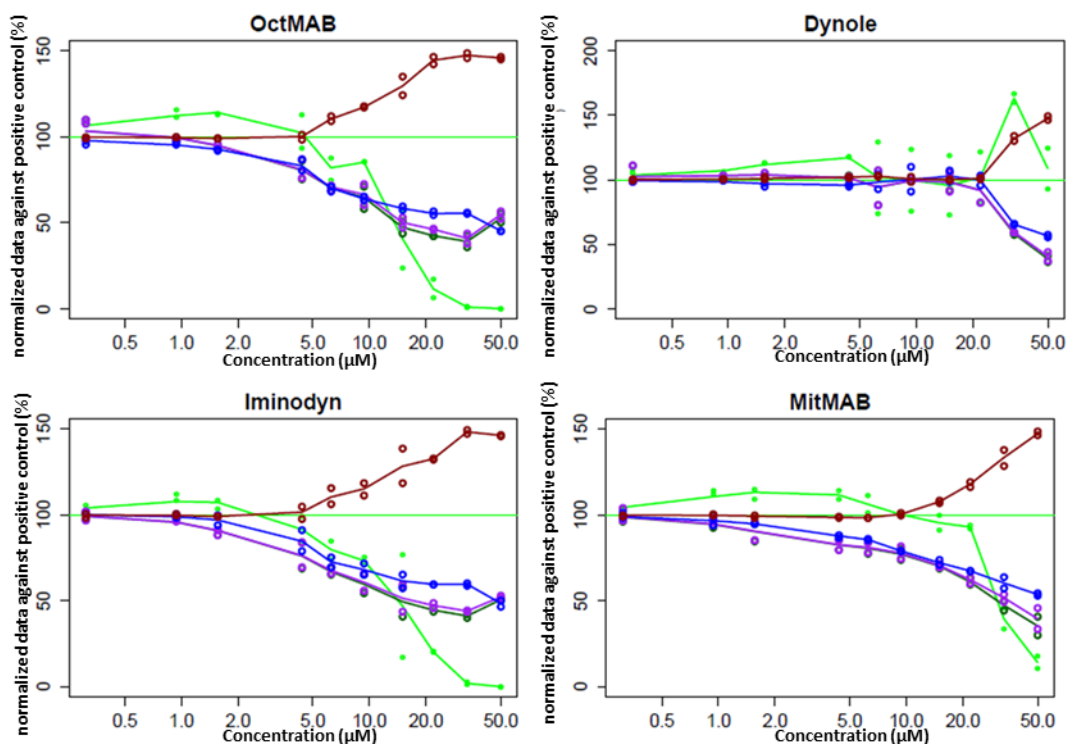


Figure 17: Dose response curves for dynamin inhibitors. Curves showed slight increase in the aggregate induction and cytotoxicity in a dose dependent manner. Red: cell circularity, violet: total cell number, dark green: green cell number, blue: cell area, light green: number of green aggregates.

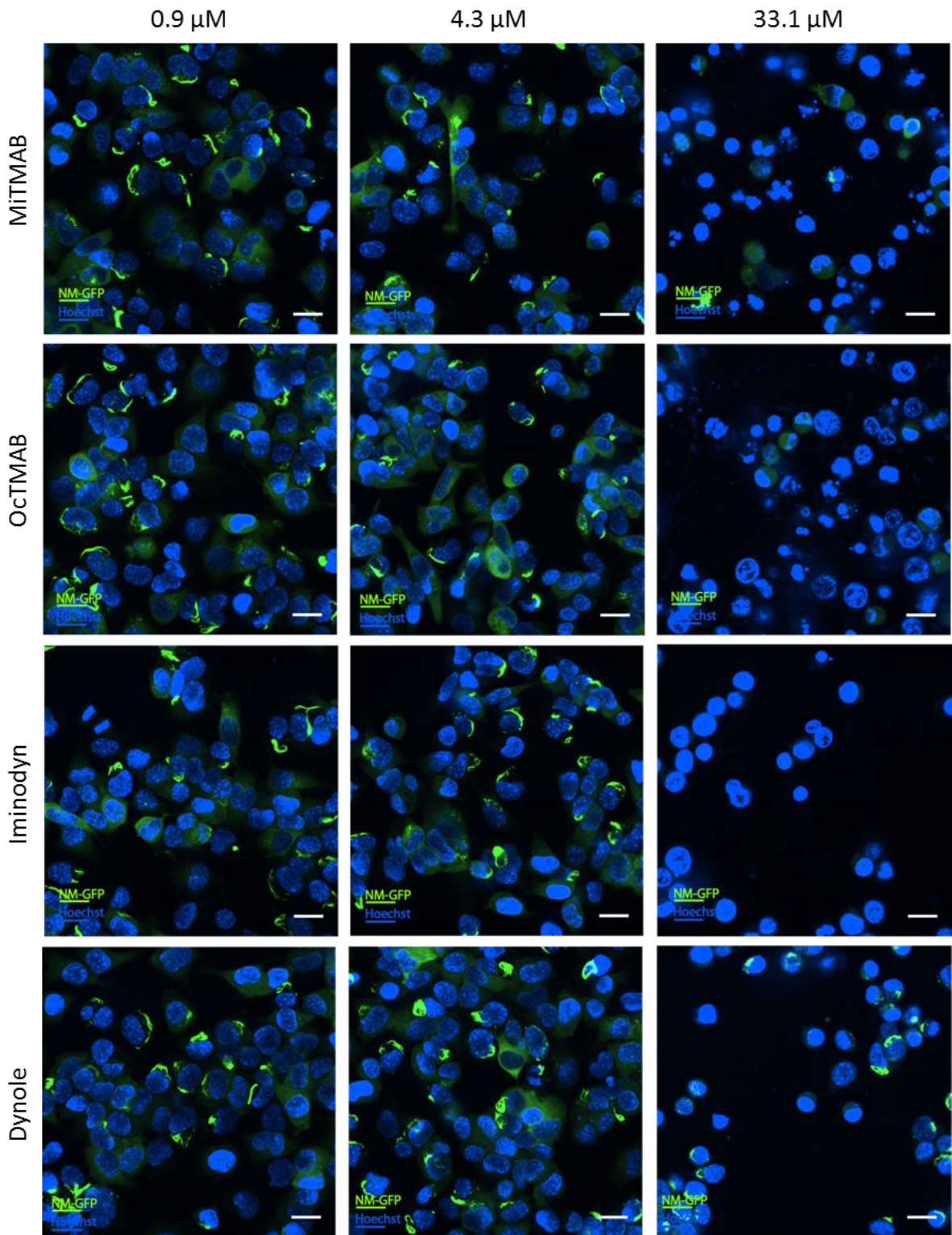


Figure 18: Cells treated with dynamin inhibitors. The first column shows cells treated with 0.9 μM , whereas the second and third column shows cells treated with 4.3 μM and 33.1 μM inhibitors, respectively. A slight increase in aggregate induction was observed especially in cell treated with MITMAB and OcTMAB (0.9 μM and 4.3 μM). Concentrations $\geq 33.1 \mu\text{M}$ are clearly cytotoxic for all compounds. Bar scale represent 20 μm .

5.2.3. Specific clathrin or caveolae inhibitors show no effect on the aggregate induction

Internalization via clathrin coated pits depends on the variety of the transmembrane receptors, their ligands and accessory molecules [47]. Complete blockade of clathrin-dependent endocytosis can be achieved by selective inhibition of the clathrin terminal domain, thereby preventing clathrin assembly [54]. For this purpose, cells were treated with pitstop1 and pitstop2, novel clathrin inhibitors, in the range of 0.8 μM to 125 μM (Figure 19) [53]. A pitstop2 negative control, which belongs to the same chemical class as pitstop2, but has no clathrin inhibitory effect, was used as a negative control for pitstop2. No change in the aggregate induction was observed with pitstop1 and pitstop2 at concentrations that did not impair cell viability.

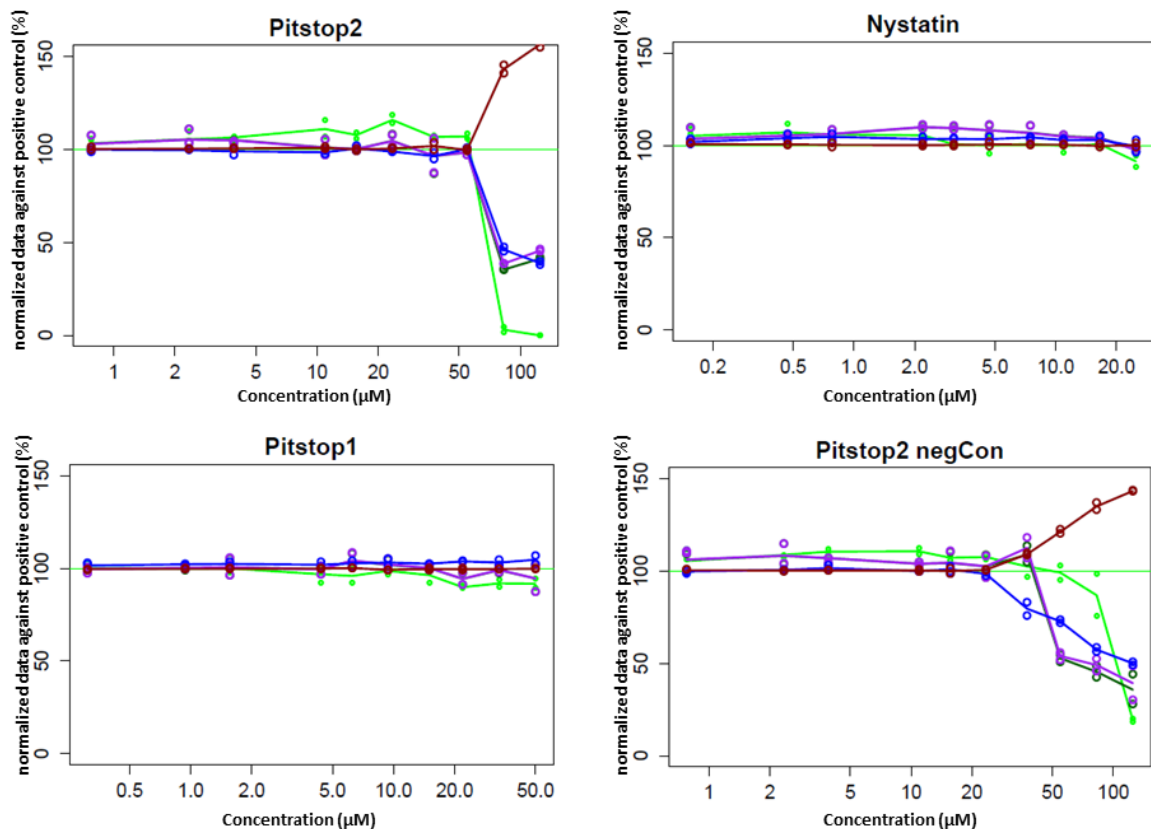


Figure 19: Dose response curves for clathrin and caveolae inhibitors. Curves showed no difference in the aggregate induction in a dose dependent manner. Red: cell circularity, violet: total cell number, dark green: green cell number, blue: cell area, light green: number of green aggregates.

Caveolae are the most known non-clathrin coated plasma membrane vesicles. Since this pathway is highly cholesterol dependent, the most efficient inhibition is depletion of intracellular cholesterol [54]. In our experiment, concentrations ranging from 0.3 μM to 50 μM of nystatin were used. This polyene antibiotic interacts with cholesterol-rich membrane areas (lipid rafts) and causes large membrane clusters, which are visible by freeze-fracture electron microscopy [54]. Cytotoxicity has been reported at increased concentrations [54]. However, our data revealed neither any effect on aggregate induction nor a cytotoxic effect of nystatin. In conclusion, our screens suggest that neither caveolae nor clathrin-coated pits alone play a dominant role in NM-GFP protein aggregate induction by exogenous NM fibrils. A possible explanation could be that the NM fibrils utilize alternative endocytic pathways to enter the cell.

5.2.4. Inhibition of macropinocytosis decreases the number of cells with induced NM-GFP protein aggregates

Several lines of evidence suggest that pathologic prion protein uptake follows macropinocytosis [45, 66]. Moreover, also SOD-1 aggregates enter cells via macropinocytosis [46]. To test whether macropinocytosis might also play a role in NM-GFP protein aggregate induction by exogenous NM fibrils, we inhibited p21-activated kinase (PAK), phosphoinositide 3-kinase (PI3K), tyrosine kinase (TK) and sodium/proton exchanger, the molecules involved in the fluid phase uptake.

Potent PAK inhibitor FRAX486 was used at concentrations between 0.3 μM and 50 μM . Interestingly, it increased the aggregate induction at lower concentrations (<2 μM), whereas it decreased the induction rate at concentrations above 2 μM (Figure 20 and 21). The effect of this PAK inhibitor at even lower concentration remains to be tested. Here we show that FRAX486, which blocks macropinocytosis, efficiently inhibits the aggregate induction in tested cells. Another PAK inhibitor, IPA-3, was also tested. Although drastically decreased induction in cells treated with concentrations above 10 μM IPA-3 was observed, the decrease strongly correlated with cytotoxicity and was thus considered unspecific. Interestingly, however, aggregate induction was before cytotoxicity effect increased for 25%.

Phosphoinositide 3-kinase (PI3K) has been shown to play an important role in macropinocytosis [67]. (PI3K) inhibitor wortmannin is widely used compound to block this process in concentrations between 0.3 μM and 50 μM [67]. As shown in Figure 20, it effectively reduced the number of cells with green aggregates, without any undesirable toxic side effects.

Macropinocytosis has also been targeted by inhibiting the sodium/proton exchanger with amiloride (EIPA) and its derivatives [54]. EIPA, a selective Na^+/H^+ antiporter inhibitor was used at concentrations ranging from 0.8 μM to 125 μM (Figure 20). Here, EIPA significantly decreased the aggregate induction at the mid-range concentrations without toxicity. Above 30 μM , EIPA showed cytotoxicity, resulting in cytoplasm condensation

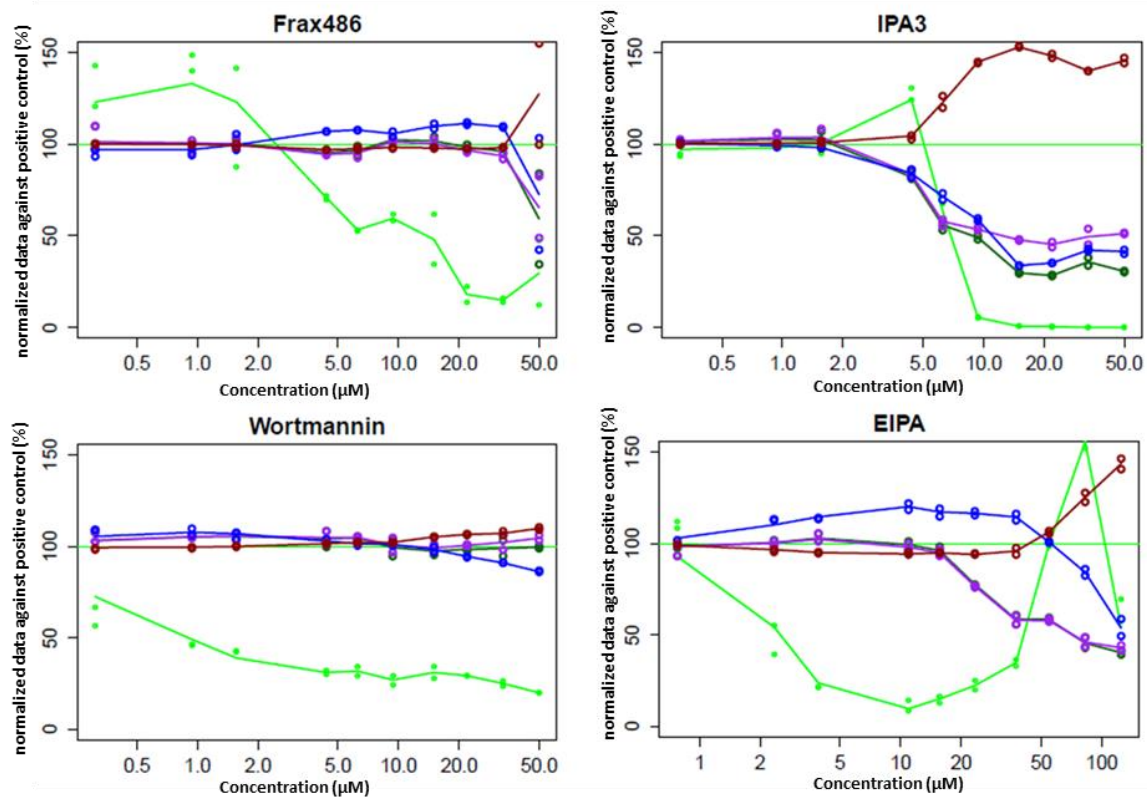


Figure 20: Dose response curves for macropinocytosis inhibitors. FRAX486 shows an interesting in- and decrease in aggregate induction. Whereas FRAX486 is not cytotoxic, another PAK inhibitor, IPA-3, shows an extreme cytotoxic effect. Wortmannin effectively blocked the aggregate induction without any observed cytotoxic effect. The EIPA dose response curve clearly shows decrease in aggregate induction. Increased green aggregates in high concentration range are a consequence of condensed cytoplasm due to cytotoxicity shown in Figure 21B. Red: cell circularity, violet: total cell number, dark green: green cell number, blue: cell area, light green: number of green aggregates.

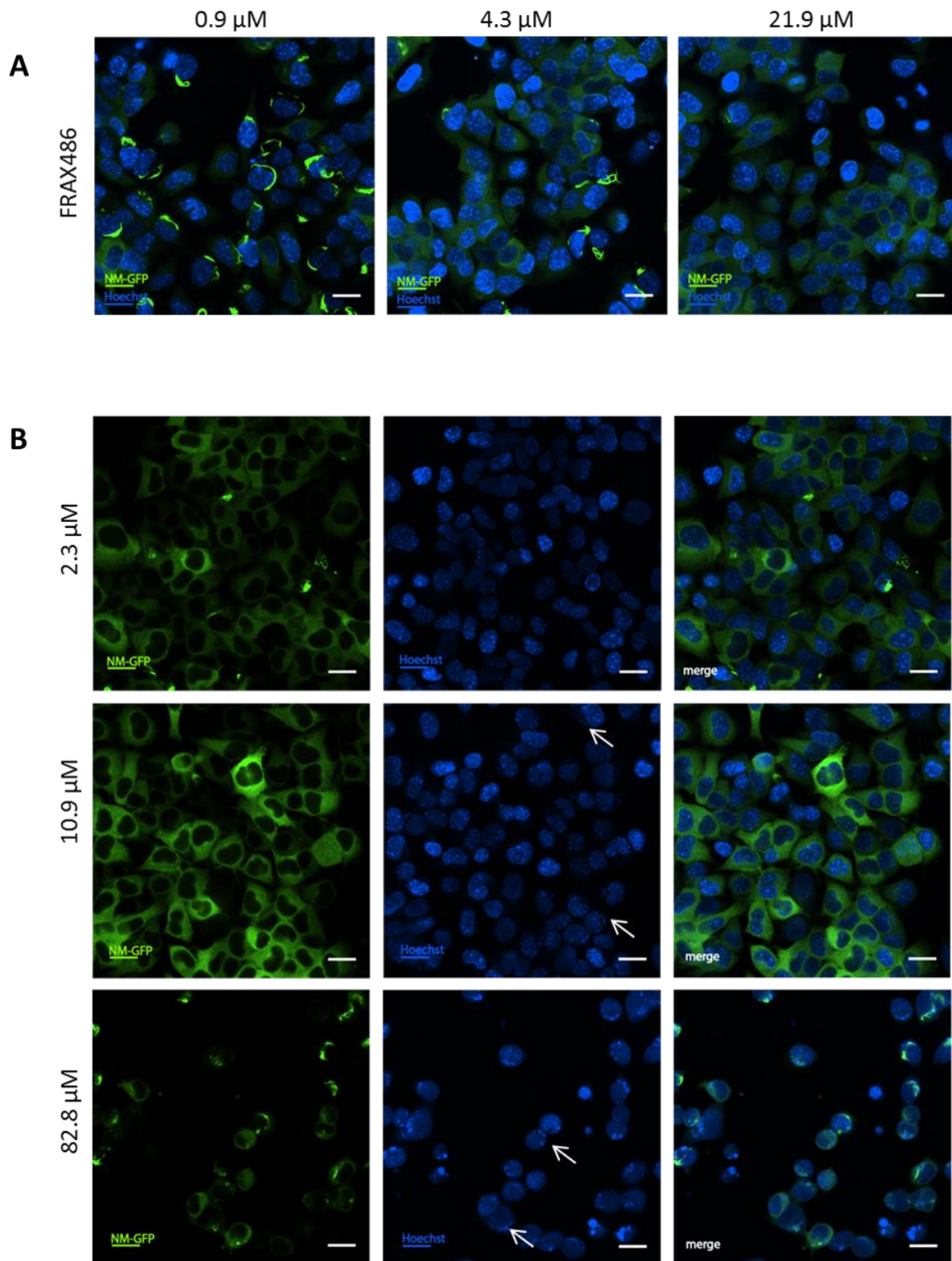


Figure 21: Cells treated with FRAX486 and EIPA. (A) FRAX486 at low concentration (0.9 μM) increased aggregate induction in NM-GFP cells, which decreased dramatically in the mid-concentration range. **(B)** At low concentrations (2.3 μM), EIPA inhibited the aggregate induction. This inhibition effect increases in a dose-dependent manner. Interestingly, upon 10 μM , cytoplasmic Hoechst stain was observed. Arrows point at the non-nuclei Hoechst staining. Bar scales represent 20 μm .

and thus increased false positive results. Furthermore, an undefined smear of Hoechst staining was observed around the nuclei area in concentrations above 10 μM . Interestingly, intensity of this stain increased parallel with the compound concentration. The reason for this Hoechst staining remains to be identified. Wortmannin in a large concentration range was found to be a very useful compound to study the impact of endocytosis since it shows no cytotoxic effect. Also EIPA, FRAX486 at concentrations ranging from 2 μM to 50 μM and from 4 μM and 20 μM respectively, did not appear to affect cell viability and were also identified as potential hits in this experiment.

Since genistein inhibits the biological activity of several tyrosine kinases it was initially used as a macropinocytosis inhibitor [68]. It was applied to the cells at concentrations between 1.6 μM and 250 μM . Our results showed no effect of genistein on the aggregate induction. However, as shown in Figure 22, it altered the induced aggregate morphology and led to mostly semi-circular aggregates compared to control with various aggregate forms. With high genistein concentrations (>50 μM), the percent of cells with green aggregates increased. This paralleled cytotoxicity, and may thus rather be unspecific (Figure 22).

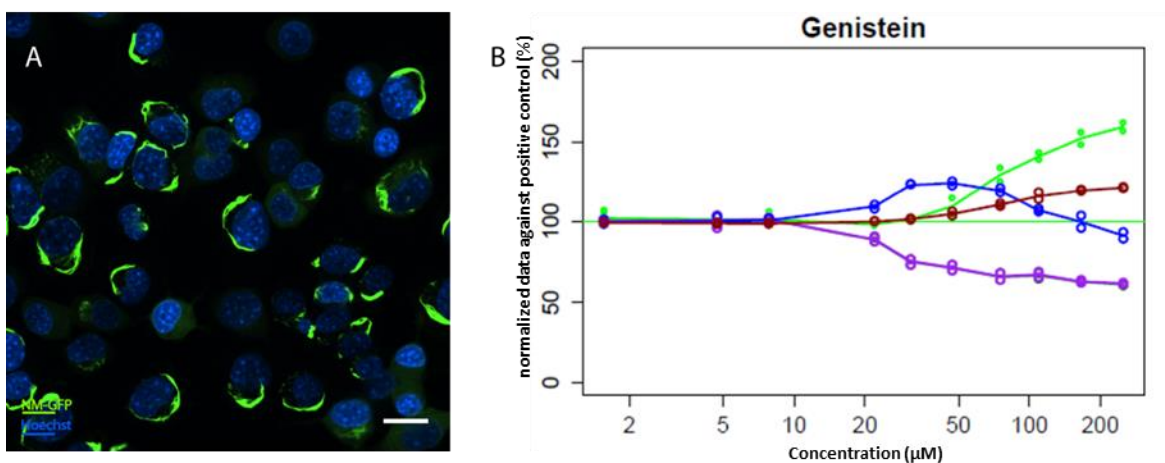


Figure 22: Cells treated with genistein. (A) Increased concentrations (165.6 μM) induce semi-circular aggregate phenotype. Bar scale represent 20 μm . (B) Dose response curve for genistein.

6 DISCUSSION

6.1 The yeast Sup35NM domain is suitable for the cell-based aggregate induction assay

Prions are proteinaceous infectious protein aggregates that can enter the cell and are able to induce the aggregation of the homotypic protein. However, the exact mechanisms of prion uptake and induction are unknown. Like mammalian prions, also yeast Sup35 protein, was shown to have prion characteristics and in its prion conformation, is able to impose its abnormal conformational state onto its cytosolic counterparts. To study this in detail, a neuroblastoma cell-based novel assay has been established. In this model, the addition of recombinant Sup35NM domain fibrils induces the aggregation of the homotypic cytosolically expressed NM-GFP protein [44]. How this is accomplished and which cellular processes are involved was unknown. The first aim of this study was to optimise the aggregate induction assay for the high content screening purpose. High content screening, also known as high content analysis is automated microscope-based screening that offers simultaneous analysis in complex biological systems to identify possible pathways or molecular targets for drug discovery. It allows a scientist to test compound libraries with a wide spectrum of biologically active compounds at once. Compound libraries consist of unique small molecules obtained from plants, animals, or microorganisms, which have been promising for new drug discovery since the beginning of modern pharmaceutical development. Even siRNA can be included in the screen to silence certain genes and reduce or completely negate the function of the corresponding protein.

Thus, in the first part, an assay with high aggregate induction rate and low inter- and intra-assay variability was developed on the 384-well format. The optimised parameters were cell seeding number and passage number, fibril working concentrations and sonication protocols. The second aim of this study was to use this well-developed system to investigate the role of endocytic pathways for cytosolic prion aggregate induction. In order to specify the endocytic pathways involved in the aggregation of the NM protein, fifteen known specific endocytic inhibitors were analysed in the screen for their effect on the aggregate induction.

6.1.1. Optimised NM fibril aggregate induction assay for high content screening

To date, prion formation, propagation and maintenance have been extensively studied in yeast. In yeast, Hsp104 has been shown to play an important role in aggregate fragmentation [56]. In mammalian cells, however no homolog for this disaggregase has yet been identified [56]. This clearly indicates that aggregate propagation in mammalian cells does not depend on this disaggregase. Krammer and colleagues have shown that *in vitro* formed recombinant yeast Sup35NM fibrils induce aggregation of the homotypic protein in the cytosol of the mammalian cells [43, 44]. In this model system, 50-60% of N2a cells expressing soluble NM-HA in the cytosol include NM-HA aggregates after the application of the NM fibrils. Additionally, it was shown that induced NM-HA aggregates fulfil all prion criteria in N2a cells. First, external seeds can induce aggregation of the homotypic precursor protein in its soluble non-prion state. Second, the induced aggregates are mitotically stable and third, can spread to the neighbouring cells. However, the exact mechanisms of the fibril internalization and aggregate induction and propagation remain unknown.

Here, we were interested in understanding if endocytic pathways are involved in aggregate induction. Thus, we designed the aggregate induction assay for high content screen using N2a cells expressing soluble NM tagged with the GFP (NM-GFP^{sol} cells). Since cells do not need to be additionally stained with the anti-HA antibody as in Krammer's protocol, this system provides us with faster and cost-effective method to study the NM fibril aggregate induction. On the other hand, the GFP tag is bigger than HA tag, which might affect the aggregate induction. However, with the optimised protocol and following strict standard operating procedures, in the optimised assay, NM fibrils induced NM-GFP protein aggregation in 40-50% cells.

6.1.2. NM fibril preparation

Sup35NM protein fibrillates *in vitro* under constant rotation [1, 25, 37, 43, 44, 55]. Rotation at different temperatures, with distinct protein rotation concentrations, volumes and size of rotating tubes produce fibrils with different conformational characteristics, which induce variable aggregates in yeast. It has been shown that NM fibrils produced at 4°C are more resistant to temperature denaturation *in vitro* and have higher infection

efficiency in yeast as the ones generated at room temperature or 37°C [42]. In our case, NM fibrils rotated at 4°C also induce higher percentage of NM-GFP^{agg} cells compared to the ones produced at the room temperature. We did not include fibrils rotated at 37°C in our experiment. If this condition produces even stronger fibrils remains to be elucidated. Several lines of evidence, including atomic force microscopy (AFM), thioflavin T assay and biochemistry methods such as temperature denaturation resistance already showed that NM fibrils produced with the rotation method are really fibrils [1, 25, 37]. The thioflavin T assay is based on spectrophotometric measurements of increased fluorescence upon its propensity to bind to the β -structures of fibrils [25]. Electron microscopy or ATM can be utilized to determine the structure of the produced fibrils and whether only one type or several conformational variants were produced.

It is believed that size and structure of fibrils are crucial for an effective cellular uptake, aggregate induction and aggregate propagation. Smaller fibril fragments might be taken up more easily into the cytosol, where they promote aggregation of homotypic soluble proteins. By the sonication process, long fibrils are most probably broken into smaller pieces [30]. In our experiment, cytosolic aggregates were efficiently induced by sonicated fibrils, which suggests that fragmented fibrils might either enter the cells more efficiently or provide more seeds to induce aggregates.

At the beginning of this study, the aggregate induction efficiency was about 5%, and after optimisation we were able to repeatedly induce aggregation in up to 40-50% of the cells. This dramatic increase indicates the importance of a suitable fibril preparation protocol and following standard operating procedures for cell culturing. Nevertheless, it cannot be excluded that some protein stocks already included fibril seeds, which would accelerate the fibrillization process and lead to selective amplification of this specific conformer (also called prion strain) that gives this high induction rate. To understand this and isolate the specific aggregate conformer, protein misfolding cyclic amplification (PMCA) method based on subsequent serial dilution-amplification cycles of the initial seeds may help [30]. Another reason of the lower induction efficiency at the beginning may be due to reduced protein concentration because of binding of the protein on the wall of non-low binding protein tubes. As we have later switched to the low-binding tubes, more protein aggregates could have been added to the cells.

6.1.3. NM-GFP protein aggregate induction

For high content screening, a robust assay with modest variation between experiments is important. Besides the fibrils, biological cell variability, different lots of frozen cell stocks and material supplements all lead to inter-assay variations in the aggregate induction rate. Thus, strict standard operating procedures are very important for a robust assay for high content screening. N2a cells origin from cancer cells, which makes this cell population susceptible to genetic abnormalities. Thus, the usage of the same proper cell passage number, standard cell cultivation and fibril treatment protocols are necessary to get constant results.

It is surprising to find that both the cell attachment time and the fibril incubation time have no influence on the percent of NM-GFP^{agg} cells. Even shortening the fibril incubation time to 12 hours instead of 24 hours did not reduce the results. These may indicate a fast aggregate formation kinetic upon NM fibril addition and the plateau is reached already within 12 hours after induction. Alternatively, aggregates might be partially degraded after 12 hours post induction.

6.2 The screen revealed interesting endocytic pathways involved in NM fibril aggregate induction

To test the reproducibility and feasibility of our assay, a screen including 15 potential compounds that block different endocytic pathways was performed twice under the same conditions. Both screens yielded the same results, showing low inter-assay variability. In yeast, prion induction with recombinant Sup35NM fibrils is very difficult and higher rate of formatted prion colonies can be reached only with the help of liposome-based method or polyethylene glycol [42]. In contrast to yeast, NM fibrils are in N2a cells internalised without extra help and induce very high percentage of NM-GFP^{agg} cells with green aggregates (50%). Our hypothesis is that NM fibrils could be taken up directly or by the active cellular endocytic processes. Clathrin-, caveolae-, dynamin-dependent pathways, and macropinocytosis are known endocytic pathways, which are involved in the internalization of variable viruses [69] and the mammalian prion protein [45, 66], respectively. These pathways were our candidate pathways that might be involved in the NM fibril uptake in N2a cells. To elucidate this, few endocytosis inhibitors were tested in

this experiment. Although the decrease or increase of aggregate induction is rather an indirect hint for decreased or increased NM fibril uptake, the involvement of the compounds in mechanisms other than fibril internalization should also be considered. The results point out the possible role of the specific pathway in NM fibril aggregate induction in our system.

6.2.1. Actin disruption reduces aggregate induction

Actin is the most important component in macropinocytosis, where the formation of large F-actin coated vacuoles serves to internalize liquid from the extracellular space. Besides its function in macropinocytosis, it has been shown that the actin cytoskeleton is also required for clathrin- and caveolae-dependent endocytosis in mammalian cells [48]. However it remains unclear, whether actin filaments are involved in coated vesicle budding or are generally responsible for structural integrity and the function of plasma membrane [63]. Additionally, Ganusova and colleagues have demonstrated that Sup35NM domain in yeast interacts with the actin cytoskeleton via multiple components [70]. Furthermore, they showed that long-term disruption of the actin machinery by latrunculin A results in a significant loss of prion phenotype, suggesting the possible link between the actin cytoskeleton and the prion formation and propagation. Thus, we were interested in whether actin disassembly affects the aggregate induction in our system, either through blocking the uptake of NM fibrils or affecting the propagation mechanisms. In our results, the strong decrease in the aggregate induction rate in the N2a cells treated with latrunculin A, cytochalasin A and D clearly indicates the importance of the actin cytoskeleton in the aggregate induction. We anticipate that the NM fibrils are unable to enter the cell, when the actin filaments are destabilized. Despite that, 20% of the NM-GFP^{agg} cells were observed, suggesting that some of the NM fibrils still enter the cell via alternative pathway. Furthermore, cells treated with actin disruptors have a tendency to cluster, building long chains including 5-30 cells, which indicate the improper cell activity.

6.2.2. Macropinocytosis is involved in aggregate induction

Our screen with either dynamin inhibitors, which block both caveolae and clathrin-dependent endocytosis, or specific inhibitors such as nystatin for caveolae and pitstop1 and pitstop2 for clathrin showed no decrease in aggregate induction. This suggested neither caveolae nor clathrin-coated pits alone play a dominant role in NM aggregate induction. Contrary, as discussed in the previous chapter, functional actin polymerisation machinery is certainly necessary for affective aggregate induction. Furthermore, the cytoskeleton is also intensively involved in membrane ruffling during macropinocytosis. The aggregate induction drastically decreased upon treatment with macropinocytosis inhibitors, such as amiloride (EIPA), FRAX486, and wortmannin. These compounds worked indirectly on macropinocytosis through ion exchangers, p21-activated kinases (PAKs), and phosphoinositide 3-kinase (PI3K), respectively.

How EIPA inhibits macropinocytosis is unclear. However, apparently Na^+/H^+ exchanger (NHE), EIPA's primary target, plays a role in this process. Some hypotheses proposed the Na^+/H^+ exchanger's impact on macropinocytosis [71]. Three hypotheses have been proposed. First, cellular uptake of the Na^+ might attract the osmotically driven water to enter, which would cause swelling and extension of macropinocytosis ruffles. Second, an increased intracellular Na^+ can promote the uptake of Ca^{2+} via $\text{Na}^+/\text{Ca}^{2+}$ exchanger, which has already been suggested to mediate macropinocytosis. Thirdly, the effect of the exchangers on the macropinocytosis could be regulated by cytosolic pH alteration. Thus, inhibition of the exchanger by EIPA hinders cells to eliminate excessive protons, causing intracellular acidification. This further results in altered signalling and/or cytoskeletal function, required for cell ruffling. In the dose response curve, EIPA blocked the aggregate induction almost completely at concentrations of 2-25 μM without any cytotoxicity, which strongly indicates the possible involvement of macropinocytosis in the aggregate induction. Interestingly, in cells treated with EIPA, a faint Hoechst staining was observed next to the nuclei, which increased concomitantly with the compound concentration. Since ion exchangers are present in all membranes, this might be the compound's effect on the nuclei membrane. Another reason might be the mitochondrial DNA, which could be condensed around the nuclei. It should not be excluded that the nuclear membrane was dysfunctional or even damaged upon higher concentration of EIPA, thus the leakage of DNA out of nuclei. To better understand the role of Na^+/H^+ exchanger, other NHE

inhibitors with different chemical structural such as DMA and MIA, which belong to the same family as EIPA, are to be tested. Additionally, compounds from the aroylguanidine family such as KR-32568 and Zoniporide are as well to be used in further experiments.

Also FRAX486 inhibition altered upon different concentrations, clearly showing the compound's effect depends on their concentration. The decrease of the aggregate induction rate upon higher FRAX486 concentrations confirms the PAK involvement in the aggregation mechanisms. Aggregate increase by lower FRAX486 concentrations is very interesting and may indicate distinct roles of different compound targets at high and low concentrations. There are two PAK groups, PAKI (PAK1-3) and PAKII (PAK4-6). PAK1 has been implicated to be involved in the formation of actin-rich ruffles via binding to its upstream activator Cdc42 [50]. It has been shown that FRAX486 inhibits the PAKI group and PAK4 proteins. IPA3 targets also only the PAKI group; however, its inhibitory effect on aggregation in our screen correlated with cytotoxicity. To further distinguish the roles of different PAKs in the aggregate induction, compounds targeting distinct PAKs like PF-03758309, the specific PAK4 inhibitor and FRAX597, the other PAKI inhibitors are to be tested.

Wortmannin is another widely used macropinocytosis inhibitor. It blocks the PI3K, which has been implied to affect different steps of growth factors signalling and intracellular vesicles trafficking, including nucleation, elongation and bundling of the actin filaments [54, 67]. This potent PI3K inhibitor is involved in actin reorganisation and plays a crucial role in vesicle formation and fusion [50, 54]. Certainly, PI3K inhibitors have pleotropic effects since they are also able to block the clathrin- and caveolae-dependent uptake of certain ligands [54]. In our experiments, wortmannin blocked the fibril uptake by more than 70%, indicating the involvement of PI3K signalling in the aggregate induction. Additionally, no changes in cell morphology or cytotoxicity were observed even at high concentrations.

EIPA, FRAX486 and wortmannin are three commonly used macropinocytosis inhibitors, affecting the endocytic pathway through different mechanisms and showing the same results in the decreased aggregate induction. Thus, macropinocytosis plays an important role during aggregate induction by exogenous NM fibrils.

6.2.3. Dynamin inhibition may up-regulate macropinocytosis

In our screen, interestingly, treatment with dynamin inhibitors revealed slight increase in the percentage of NM-GFP^{agg} cells. Dynamin is involved in both clathrin- and caveolae-dependent pathways, blockade of which did not negatively affect the aggregate induction but rather increased the induction rate. Concomitantly, clathrin assembly inhibitors (pitstop1 and pitstop2) alone did not affect the aggregate induction. Similarly, nystatin, which inhibits the caveolae pathway through distortion of the cholesterol-rich membrane, also did not show any inhibition or activation effect. Since dynamin regulates vesicle scission and is involved in several endocytic pathways, including the clathrin- and caveolae-dependent pathways, it might be that inhibition of both major endocytic pathways leads to a compensatory effect and thus the increased third major pathway, the macropinocytosis. To confirm our hypothesis, fluorescently labelled dextran, transferrin and cholera toxin, which are the most commonly used markers for macropinocytosis, clathrin-dependent and caveolae-dependent pathways, respectively, are to be used in combination with the dynamin inhibitors. Decrease in the signal of transferrin and cholera toxin accompanied with increase in the dextran will be a strong hint to indicate the different regulatory effect on endocytic pathways of the compounds.

6.2.4. Genistein affects the morphology of the induced NM-GFP protein aggregates

In vitro generated NM fibrils can form multiple fibril types [43]. In our model system, also various morphological aggregate phenotypes were observed. Some aggregates were large and spindle-shaped, whereas others appeared as puncta. Cells with similar aggregate phenotypes were possibly localized next to each other in the wells, suggesting they were progeny and thus that the aggregate phenotype was inherited. Furthermore, that would imply that Sup35NM aggregates can either inherit their variant characteristics upon transmission or give rise to new phenotypes. Interestingly, genistein induced one specific semicircular phenotype, suggesting that only a certain fibril strain was able to enter the cell. Genistein is a phytoestrogen affecting various systems. It has been shown to inhibit tyrosine kinases, which would indirectly block the macropinocytosis, while in some other studies it has been determined as caveolae inhibitor [72]. Due to these findings it is difficult to define the genistein's main target in our model system.

6.3 Relevance of this study

Pathologic protein aggregation by a seeded polymerization process is also a hallmark of many neurodegenerative diseases of humans. The aggregated proteins in Alzheimer's disease, Parkinson's disease and other age-related neurodegenerative diseases are also associated with formation of aggregating proteins, which share several characteristics with prions [23, 29]. Structural analysis showed that not only the PrP, but also many distinct misfolded proteins are assembled into highly ordered fibrils with high content of β -structures, termed amyloids. Recent discoveries suggest that Tau, α -synuclein, and other proteins involved in neurodegenerative diseases might propagate their amyloid state in a prion-like manner within diseased organs [73, 74]. Braak and colleagues suggested that protein aggregation spreads in predictable patterns along anatomically connected brain regions [29, 75]. Interestingly, however, post mortem examination of the brain 16 years after transplantation of fetal brain tissue into Parkinson's patients showed aggregates in grafted cells, suggesting that the disease was able to spread to young neurons [76]. These findings suggest the existence of a common mechanism in the spreading of neurodegenerative disease related protein aggregates in tissues and heighten the need for further investigation for protein aggregate neuron-to-neuron transmission. Several studies have demonstrated cell-to-cell transfer of protein aggregates, but still little is known about mechanisms by which misfolded proteins are released or taken up [77-79]. Interestingly, the uptake of PrP^{Sc} also appears to depend on macropinocytosis [45]. Similar to mammalian prions, also some prion-like aggregates such as mutant superoxide dismutase-1 (SOD-1) aggregates have been proposed to be internalised via macropinocytosis [46]. This suggests that our protein shares some characteristics with proteins involved in distinct neurodegenerative diseases that spread in a prion-like manner.

7 CONCLUSION

In the first part of this study an assay with high aggregate induction rate and low inter- and intra-assay variability was developed on the 384-well format. Initially, in our cellular model, fibrils were able to induce aggregates only in 5% of the NM-GFP cells. The optimised parameters were cell seeding number and passage number, fibril working concentrations and sonication protocols. After the method optimisation we were able to induce aggregates in 50% of the cells. This clearly indicates that our aggregate induction assay optimisation was successful. In the second part we investigated the role of endocytic pathways for cytosolic prion aggregate induction. In order to specify the endocytic pathways involved in the aggregation of the NM protein, fifteen known specific endocytic inhibitors were analysed in the screen for their effect on the aggregate induction. The endocytosis screen revealed endocytic pathways that have an impact on aggregate induction in NM-GFP^{sol} cells. The aggregate induction rate was not negatively affected by clathrin- or caveolae inhibition. Since macropinocytosis inhibitors wortmannin, EIPA and FRAX486 drastically decreased aggregation, these results suggest NM aggregate induction depends on the fluid-phase uptake.

Wortmannin, FRAX486 and EIPA are three best hits from our screen. They are also the commonly used macropinocytosis inhibitors. To confirm our results that NM fibrils are taken up majorly via macropinocytosis, several further approaches are to be done. First, fluorescently labelled endocytic markers are available to trace the intracellular endocytic pathway. Fluorescently labelled dextran, transferrin and cholera toxin are the most commonly used markers for macropinocytosis, clathrin-dependent and caveolae-dependent pathways, respectively. These markers will be used in combination with our hits to visualize the compound's effects. Secondly, to visualize the NM fibrils, the protein should be labelled with a fluorescent dye using commercial labelling kits. With labelled fibrils, different approaches can be followed, such as life imaging to trace the internalization of the fibrils and a mathematical model of fibril uptake and induction kinetics can be established to study this in detail. Moreover, the effect of the macropinocytosis inhibitors on the internalization of the fibrils can be directly analysed, and the possible co-localization of the macropinocytosis markers like dextran, Lucifer yellow or horse radish peroxidase can be assessed. Furthermore, cargo uptake by macropinocytosis causes actin cytoskeletal rearrangements to form membrane ruffles [47, 48]. This can be visualized by transfecting the cells with the plasmid containing gene for lifeAct-TagRFP, a 17 aa long

peptide fused with the red fluorescent protein [80]. The visualization of actin ruffles surrounding the labelled fibrils will be a strong hint pointing out that the NM fibrils enter the N2a cells via macropinocytosis.

8 REFERENCES

1. Osherovich, L.Z., et al., *Dissection and design of yeast prions*. PLoS Biol, 2004. **2**(4): p. E86.
2. Prusiner, S.B., et al., *Prion protein biology*. Cell, 1998. **93**(3): p. 337-48.
3. Prusiner, S.B., *Novel proteinaceous infectious particles cause scrapie*. Science, 1982. **216**(4542): p. 136-44.
4. Gajdusek, D.C., *Unconventional viruses and the origin and disappearance of kuru*. Science, 1977. **197**(4307): p. 943-60.
5. Weissmann, C., *A 'unified theory' of prion propagation*. Nature, 1991. **352**(6337): p. 679-83.
6. Somerville, R.A., et al., *Biochemical typing of scrapie strains*. Nature, 1997. **386**(6625): p. 564.
7. Telling, G.C., et al., *Evidence for the conformation of the pathologic isoform of the prion protein enciphering and propagating prion diversity*. Science, 1996. **274**(5295): p. 2079-82.
8. Prusiner, S.B., *Prions*. Proc Natl Acad Sci U S A, 1998. **95**(23): p. 13363-83.
9. Dobson, C.M., *Protein misfolding, evolution and disease*. Trends Biochem Sci, 1999. **24**(9): p. 329-32.
10. Krauss, S. and I. Vorberg, *Prions Ex Vivo: What Cell Culture Models Tell Us about Infectious Proteins*. Int J Cell Biol, 2013. **2013**: p. 704546.
11. Mabbott, N.A. and G.G. MacPherson, *Prions and their lethal journey to the brain*. Nat Rev Microbiol, 2006. **4**(3): p. 201-11.
12. Hilton, D.A., et al., *Prion immunoreactivity in appendix before clinical onset of variant Creutzfeldt-Jakob disease*. Lancet, 1998. **352**(9129): p. 703-4.
13. Moore, R.A., I. Vorberg, and S.A. Priola, *Species barriers in prion diseases--brief review*. Arch Virol Suppl, 2005(19): p. 187-202.
14. Gambetti, P., et al., *A novel human disease with abnormal prion protein sensitive to protease*. Ann Neurol, 2008. **63**(6): p. 697-708.
15. Aguzzi, A. and M. Heikenwalder, *Pathogenesis of prion diseases: current status and future outlook*. Nat Rev Microbiol, 2006. **4**(10): p. 765-75.
16. Prusiner, S.B., *Molecular biology of prion diseases*. Science, 1991. **252**(5012): p. 1515-22.
17. Bian, J., et al., *Cell-based quantification of chronic wasting disease prions*. J Virol, 2010. **84**(16): p. 8322-6.

18. Bessen, R.A. and R.F. Marsh, *Identification of two biologically distinct strains of transmissible mink encephalopathy in hamsters*. J Gen Virol, 1992. **73 (Pt 2)**: p. 329-34.
19. Gough, K.C. and B.C. Maddison, *Prion transmission: prion excretion and occurrence in the environment*. Prion, 2010. **4(4)**: p. 275-82.
20. Westergard, L., H.M. Christensen, and D.A. Harris, *The cellular prion protein (PrP(C)): its physiological function and role in disease*. Biochim Biophys Acta, 2007. **1772(6)**: p. 629-44.
21. Poggiolini, I., D. Saverioni, and P. Parchi, *Prion Protein Misfolding, Strains, and Neurotoxicity: An Update from Studies on Mammalian Prions*. Int J Cell Biol, 2013. **2013**: p. 910314.
22. Colby, D.W. and S.B. Prusiner, *Prions*. Cold Spring Harb Perspect Biol, 2011. **3(1)**: p. a006833.
23. Chiti, F. and C.M. Dobson, *Protein misfolding, functional amyloid, and human disease*. Annu Rev Biochem, 2006. **75**: p. 333-66.
24. Prusiner, S.B., et al., *Scrapie prions aggregate to form amyloid-like birefringent rods*. Cell, 1983. **35(2 Pt 1)**: p. 349-58.
25. Chen, C.Y., et al., *Characterization and enzymatic degradation of Sup35^{NM}, a yeast prion-like protein*. Protein Sci, 2005. **14(9)**: p. 2228-35.
26. Come, J.H., P.E. Fraser, and P.T. Lansbury, Jr., *A kinetic model for amyloid formation in the prion diseases: importance of seeding*. Proc Natl Acad Sci U S A, 1993. **90(13)**: p. 5959-63.
27. Knowles, T.P., et al., *An analytical solution to the kinetics of breakable filament assembly*. Science, 2009. **326(5959)**: p. 1533-7.
28. Orgel, L.E., *Prion replication and secondary nucleation*. Chem Biol, 1996. **3(6)**: p. 413-4.
29. Jucker, M. and L.C. Walker, *Self-propagation of pathogenic protein aggregates in neurodegenerative diseases*. Nature, 2013. **501(7465)**: p. 45-51.
30. Soto, C., G.P. Saborio, and L. Anderes, *Cyclic amplification of protein misfolding: application to prion-related disorders and beyond*. Trends Neurosci, 2002. **25(8)**: p. 390-4.
31. Grassmann, A., et al., *Cellular aspects of prion replication in vitro*. Viruses, 2013. **5(1)**: p. 374-405.
32. Wickner, R.B., et al., *Prions in Saccharomyces and Podospora spp.: protein-based inheritance*. Microbiol Mol Biol Rev, 1999. **63(4)**: p. 844-61, table of contents.
33. True, H.L. and S.L. Lindquist, *A yeast prion provides a mechanism for genetic variation and phenotypic diversity*. Nature, 2000. **407(6803)**: p. 477-83.

34. Ter-Avanesyan, M.D., et al., *The SUP35 omnipotent suppressor gene is involved in the maintenance of the non-Mendelian determinant [psi+] in the yeast Saccharomyces cerevisiae*. Genetics, 1994. **137**(3): p. 671-6.
35. Tanaka, M., et al., *The physical basis of how prion conformations determine strain phenotypes*. Nature, 2006. **442**(7102): p. 585-9.
36. Glover, J.R., et al., *Self-seeded fibers formed by Sup35, the protein determinant of [PSI+], a heritable prion-like factor of S. cerevisiae*. Cell, 1997. **89**(5): p. 811-9.
37. Kabani, M. and R. Melki, *Yeast prions assembly and propagation: contributions of the prion and non-prion moieties and the nature of assemblies*. Prion, 2011. **5**(4): p. 277-84.
38. DePace, A.H., et al., *A critical role for amino-terminal glutamine/asparagine repeats in the formation and propagation of a yeast prion*. Cell, 1998. **93**(7): p. 1241-52.
39. Krammer, C., H.M. Schatzl, and I. Vorberg, *Prion-like propagation of cytosolic protein aggregates: insights from cell culture models*. Prion, 2009. **3**(4): p. 206-12.
40. DePace, A.H. and J.S. Weissman, *Origins and kinetic consequences of diversity in Sup35 yeast prion fibers*. Nat Struct Biol, 2002. **9**(5): p. 389-96.
41. Winkler, J., et al., *Hsp70 targets Hsp100 chaperones to substrates for protein disaggregation and prion fragmentation*. J Cell Biol, 2012. **198**(3): p. 387-404.
42. Tanaka, M., et al., *Conformational variations in an infectious protein determine prion strain differences*. Nature, 2004. **428**(6980): p. 323-8.
43. Krammer, C., et al., *The yeast Sup35NM domain propagates as a prion in mammalian cells*. Proc Natl Acad Sci U S A, 2009. **106**(2): p. 462-7.
44. Hofmann, J.P., et al., *Cell-to-cell propagation of infectious cytosolic protein aggregates*. Proc Natl Acad Sci U S A, 2013. **110**(15): p. 5951-6.
45. Wadia, J.S., et al., *Pathologic prion protein infects cells by lipid-raft dependent macropinocytosis*. PLoS One, 2008. **3**(10): p. e3314.
46. Munch, C., J. O'Brien, and A. Bertolotti, *Prion-like propagation of mutant superoxide dismutase-1 misfolding in neuronal cells*. Proc Natl Acad Sci U S A, 2011. **108**(9): p. 3548-53.
47. Doherty, G.J. and H.T. McMahon, *Mechanisms of endocytosis*. Annu Rev Biochem, 2009. **78**: p. 857-902.
48. Engqvist-Goldstein, A.E. and D.G. Drubin, *Actin assembly and endocytosis: from yeast to mammals*. Annu Rev Cell Dev Biol, 2003. **19**: p. 287-332.
49. Kiss, A.L., *Caveolae and the regulation of endocytosis*. Adv Exp Med Biol, 2012. **729**: p. 14-28.
50. Dharmawardhane, S., et al., *Regulation of macropinocytosis by p21-activated kinase-1*. Mol Biol Cell, 2000. **11**(10): p. 3341-52.

51. Cardelli, J., *Phagocytosis and macropinocytosis in Dictyostelium: phosphoinositide-based processes, biochemically distinct*. Traffic, 2001. **2**(5): p. 311-20.
52. Ridley, A.J., et al., *The small GTP-binding protein rac regulates growth factor-induced membrane ruffling*. Cell, 1992. **70**(3): p. 401-10.
53. von Kleist, L., et al., *Role of the clathrin terminal domain in regulating coated pit dynamics revealed by small molecule inhibition*. Cell, 2011. **146**(3): p. 471-84.
54. Ivanov, A.I., *Pharmacological inhibition of endocytic pathways: is it specific enough to be useful?* Methods Mol Biol, 2008. **440**: p. 15-33.
55. Chernoff, Y.O., S.M. Uptain, and S.L. Lindquist, *Analysis of prion factors in yeast*. Methods Enzymol, 2002. **351**: p. 499-538.
56. Chernoff, Y.O., et al., *Role of the chaperone protein Hsp104 in propagation of the yeast prion-like factor [psi+]*. Science, 1995. **268**(5212): p. 880-4.
57. Cenedella, R.J., *Cholesterol synthesis inhibitor U18666A and the role of sterol metabolism and trafficking in numerous pathophysiological processes*. Lipids, 2009. **44**(6): p. 477-87.
58. Bryant, D.M., et al., *EGF induces macropinocytosis and SNX1-modulated recycling of E-cadherin*. J Cell Sci, 2007. **120**(Pt 10): p. 1818-28.
59. Poh, M.K., et al., *U18666A, an intra-cellular cholesterol transport inhibitor, inhibits dengue virus entry and replication*. Antiviral Res, 2012. **93**(1): p. 191-8.
60. Misinzo, G., P.L. Delputte, and H.J. Nauwynck, *Inhibition of endosome-lysosome system acidification enhances porcine circovirus 2 infection of porcine epithelial cells*. J Virol, 2008. **82**(3): p. 1128-35.
61. Collins, S.R., et al., *Mechanism of prion propagation: amyloid growth occurs by monomer addition*. PLoS Biol, 2004. **2**(10): p. e321.
62. Phuc, H.P., J. Junwon, and C.B. Niels, *Using 96-well tissue culture polystyrene plates and a fluorescence plate reader as tools to study the survival and inactivation of viruses on surfaces*. Cytotechnology, 2011. **63**: p. 385–397.
63. Lamaze, C., et al., *The actin cytoskeleton is required for receptor-mediated endocytosis in mammalian cells*. J Biol Chem, 1997. **272**(33): p. 20332-5.
64. Sandgren, K.J., et al., *A differential role for macropinocytosis in mediating entry of the two forms of vaccinia virus into dendritic cells*. PLoS Pathog, 2010. **6**(4): p. e1000866.
65. Quan, A., et al., *Myristyl trimethyl ammonium bromide and octadecyl trimethyl ammonium bromide are surface-active small molecule dynamin inhibitors that block endocytosis mediated by dynamin I or dynamin II*. Mol Pharmacol, 2007. **72**(6): p. 1425-39.

66. Magzoub, M., et al., *N-terminal peptides from unprocessed prion proteins enter cells by macropinocytosis*. *Biochem Biophys Res Commun*, 2006. **348**(2): p. 379-85.
67. Araki, N., M.T. Johnson, and J.A. Swanson, *A role for phosphoinositide 3-kinase in the completion of macropinocytosis and phagocytosis by macrophages*. *J Cell Biol*, 1996. **135**(5): p. 1249-60.
68. Um, S.H., D.K. Rhee, and S. Pyo, *Involvement of protein kinase C and tyrosin kinase in tumoricidal activation of macrophage induced by Streptococcus pneumoniae type II capsular polysaccharide*. *Int Immunopharmacol*, 2002. **2**(1): p. 129-37.
69. Lim, J.P. and P.A. Gleeson, *Macropinocytosis: an endocytic pathway for internalising large gulps*. *Immunol Cell Biol*, 2011. **89**(8): p. 836-43.
70. Ganusova, E.E., et al., *Modulation of prion formation, aggregation, and toxicity by the actin cytoskeleton in yeast*. *Mol Cell Biol*, 2006. **26**(2): p. 617-29.
71. Koivusalo, M., et al., *Amiloride inhibits macropinocytosis by lowering submembranous pH and preventing Rac1 and Cdc42 signaling*. *J Cell Biol*, 2010. **188**(4): p. 547-63.
72. Kumano-Kuramochi, M., et al., *Lectin-like oxidized LDL receptor-1 is palmitoylated and internalizes ligands via caveolae/raft-dependent endocytosis*. *Biochem Biophys Res Commun*, 2013. **434**(3): p. 594-9.
73. Ding, F., J.J. LaRocque, and N.V. Dokholyan, *Direct observation of protein folding, aggregation, and a prion-like conformational conversion*. *J Biol Chem*, 2005. **280**(48): p. 40235-40.
74. Eisenberg, D. and M. Jucker, *The amyloid state of proteins in human diseases*. *Cell*, 2012. **148**(6): p. 1188-203.
75. Braak, H. and E. Braak, *Staging of Alzheimer's disease-related neurofibrillary changes*. *Neurobiol Aging*, 1995. **16**(3): p. 271-8; discussion 278-84.
76. Li, J.Y., et al., *Lewy bodies in grafted neurons in subjects with Parkinson's disease suggest host-to-graft disease propagation*. *Nat Med*, 2008. **14**(5): p. 501-3.
77. Mohamed, N.V., et al., *Spreading of tau pathology in Alzheimer's disease by cell-to-cell transmission*. *Eur J Neurosci*, 2013. **37**(12): p. 1939-48.
78. Brundin, P., R. Melki, and R. Kopito, *Prion-like transmission of protein aggregates in neurodegenerative diseases*. *Nat Rev Mol Cell Biol*, 2010. **11**(4): p. 301-7.
79. Narkiewicz, J., G. Giachin, and G. Legname, *In vitro aggregation assays for the characterization of alpha-synuclein prion-like properties*. *Prion*, 2014. **8**(1).
80. Riedl, J., et al., *Lifeact: a versatile marker to visualize F-actin*. *Nature methods*, 2008. **5**(7): p. 605.